

# 1 **Plastid phylogenomics reveals evolutionary relationships in the** 2 **mycoheterotrophic orchid genus *Dipodium* and provides** 3 **insights into plastid gene degeneration**

4  
5 **Stephanie Goedderz<sup>1,2,\*</sup>, Mark A. Clements<sup>3</sup>, Stephen J. Bent<sup>4</sup>, James A. Nicholls<sup>5</sup>,**  
6 **Vidushi S. Patel<sup>6</sup>, Darren M. Crayn<sup>1</sup>, Philipp M. Schlüter<sup>2</sup>, Katharina Nargar<sup>1,6,\*</sup>**  
7

8 <sup>1</sup> Australian Tropical Herbarium, James Cook University, PO Box 6811, Cairns, QLD 4870,  
9 Australia.

10 <sup>2</sup> Department of Plant Evolutionary Biology, Institute of Biology, University of Hohenheim,  
11 Stuttgart, Germany.

12 <sup>3</sup> Centre for Australian National Biodiversity Research (joint venture between Parks Australia  
13 and CSIRO), GPO Box 1700, Canberra, ACT 2601, Australia.

14 <sup>4</sup> Data61, Commonwealth Industrial and Scientific Research Organisation (CSIRO), GPO Box  
15 2583, Brisbane, QLD 4001, Australia.

16 <sup>5</sup> Australian National Insect Collection, Commonwealth Industrial and Scientific Research  
17 Organisation (CSIRO), GPO Box 1700, Canberra, ACT 2601, Australia.

18 <sup>6</sup> National Research Collections Australia, Commonwealth Industrial and Scientific Research  
19 Organisation (CSIRO), GPO Box 1700, Canberra, ACT 2601, Australia.

## 20 21 **\* Correspondence:**

22 Stephanie Goedderz  
23 [stephanie.goedderz@jcu.edu.au](mailto:stephanie.goedderz@jcu.edu.au)  
24 Katharina Nargar  
25 [katharina.nargar@csiro.au](mailto:katharina.nargar@csiro.au)

26 **Keywords:** *Dipodium*, divergence-time estimation, gene degradation, mycoheterotrophy,  
27 phylogenetics, plastome

## 28 **Abstract**

29 The orchid genus *Dipodium* R.Br. (Epidendroideae) comprises leafy autotrophic and leafless  
30 mycoheterotrophic species, the latter confined to sect. *Dipodium*. This study examined  
31 plastome degeneration in *Dipodium* in a phylogenomic and temporal context. Whole plastomes  
32 were reconstructed and annotated for 24 *Dipodium* samples representing 14 species and two  
33 putatively new species, encompassing over 80% of species diversity in sect. *Dipodium*.  
34 Phylogenomic analysis based on 68 plastid loci including a broad outgroup sampling across

35 Orchidaceae found sect. *Leopardanthus* as sister lineage to sect. *Dipodium*. *Dipodium*  
36 *ensifolium*, the only leafy autotrophic species in sect. *Dipodium* was found sister to all leafless,  
37 mycoheterotrophic species, supporting a single evolutionary origin of mycoheterotrophy in the  
38 genus. Divergence time estimations found that *Dipodium* arose ca. 33.3 Ma near the lower  
39 boundary of the Oligocene and crown diversification commenced in the late Miocene, ca. 11.3  
40 Ma. Mycoheterotrophy in the genus was estimated to have evolved in the late Miocene, ca. 7.3  
41 Ma, in sect. *Dipodium*. The comparative assessment of plastome structure and gene degradation  
42 in *Dipodium* revealed that plastid *ndh* genes were pseudogenised or physically lost in all  
43 *Dipodium* species, including in leafy autotrophic species of both *Dipodium* sections. Levels of  
44 plastid *ndh* gene degradation were found to vary among species as well as within species,  
45 providing evidence of relaxed selection for retention of the NADH dehydrogenase complex  
46 within the genus. *Dipodium* exhibits an early stage of plastid genome degradation as all species  
47 were found to have retained a full set of functional photosynthesis-related genes and  
48 housekeeping genes. This study provides important insights into plastid genome degradation  
49 along the transition from autotrophy to mycoheterotrophy in a phylogenomic and temporal  
50 context.

## 51 **1 Introduction**

52 Heterotrophic plants - plants that rely on other organisms for energy and nutrients - are  
53 remarkable survivors, exhibiting often curious morphological, physical, or genomic  
54 modifications, reflecting evolutionary relaxed selective pressure on photosynthetic function  
55 (Graham et al., 2017; Barrett et al., 2019). Advances in next generation sequencing and  
56 bioinformatic pipelines have vastly accelerated the characterisation of plastid genomes  
57 (plastomes), including of heterotrophic plants, providing new insights into plastome evolution.  
58 Plastomes of heterotrophic plants often exhibit greatly altered structure and gene content due  
59 to photosynthesis-related genes that are no longer required (Delannoy et al., 2011; Barrett et  
60 al., 2014; Lam et al., 2015; Graham et al., 2017; Braukmann et al., 2017; Barrett et al., 2018;  
61 Wicke and Neumann 2018; Qu et al., 2019; Barrett et al., 2019; Klimpert et al., 2022; Peng et  
62 al., 2022; Wen et al., 2022). Hence, heterotrophic plants offer excellent opportunities to gain  
63 insight into plastome evolution under relaxed selection.

64 Early non-phylogenomic studies on plastome evolution in heterotrophic plants allowed the  
65 discovery of large-scale plastome evolutionary patterns and, moreover, stimulated research into  
66 fine-scale, phylogenetic comparative approaches (e.g., Delannoy et al., 2011; Logacheva et al.,  
67 2011; Roma et al., 2018). Thus far, most phylogenetic comparative studies included plastomes  
68 of taxa scattered across families, tribes, or genera (e.g., Kim et al., 2015; Feng et al., 2016; Niu  
69 et al., 2017; Lallemand et al., 2019; Li et al., 2020; Kim et al., 2020; Tu et al., 2021; Kim et  
70 al., 2023). Yet, phylogenetic, comparative approaches at infrageneric level are still scarce (e.g.,  
71 Barrett et al., 2018; Barrett et al., 2019).

72 Orchidaceae, one of the two largest flowering plant families, has undergone a greater number  
73 of independent transitions from autotrophy to heterotrophy than any other land plant lineage  
74 (Merckx 2013; Christenhusz and Byng 2016; Jacquemyn and Merckx 2019). The family  
75 comprises several heterotrophic orchid lineages which rely to some extent on mycorrhizal fungi  
76 for carbon and other nutrients i.e., initial, partial, or full mycoheterotrophy (Merckx 2013).

77 So far, most examined mycoheterotrophic orchid plastomes exhibited degradation patterns  
78 similar to those found in heterotrophic plastomes of other plants. These include a reduction in  
79 genome size, decrease in guanine-cytosine (GC) content, rearrangements, pseudogenisations  
80 and gene losses (e.g., Delannoy et al., 2011; Barrett et al., 2018; Lallemand et al., 2019; Barrett  
81 et al., 2019; Wen et al., 2022). Moreover, whole plastome sequencing has revealed patterns of  
82 plastid gene degradation for various heterotrophic plastomes which led to the development of

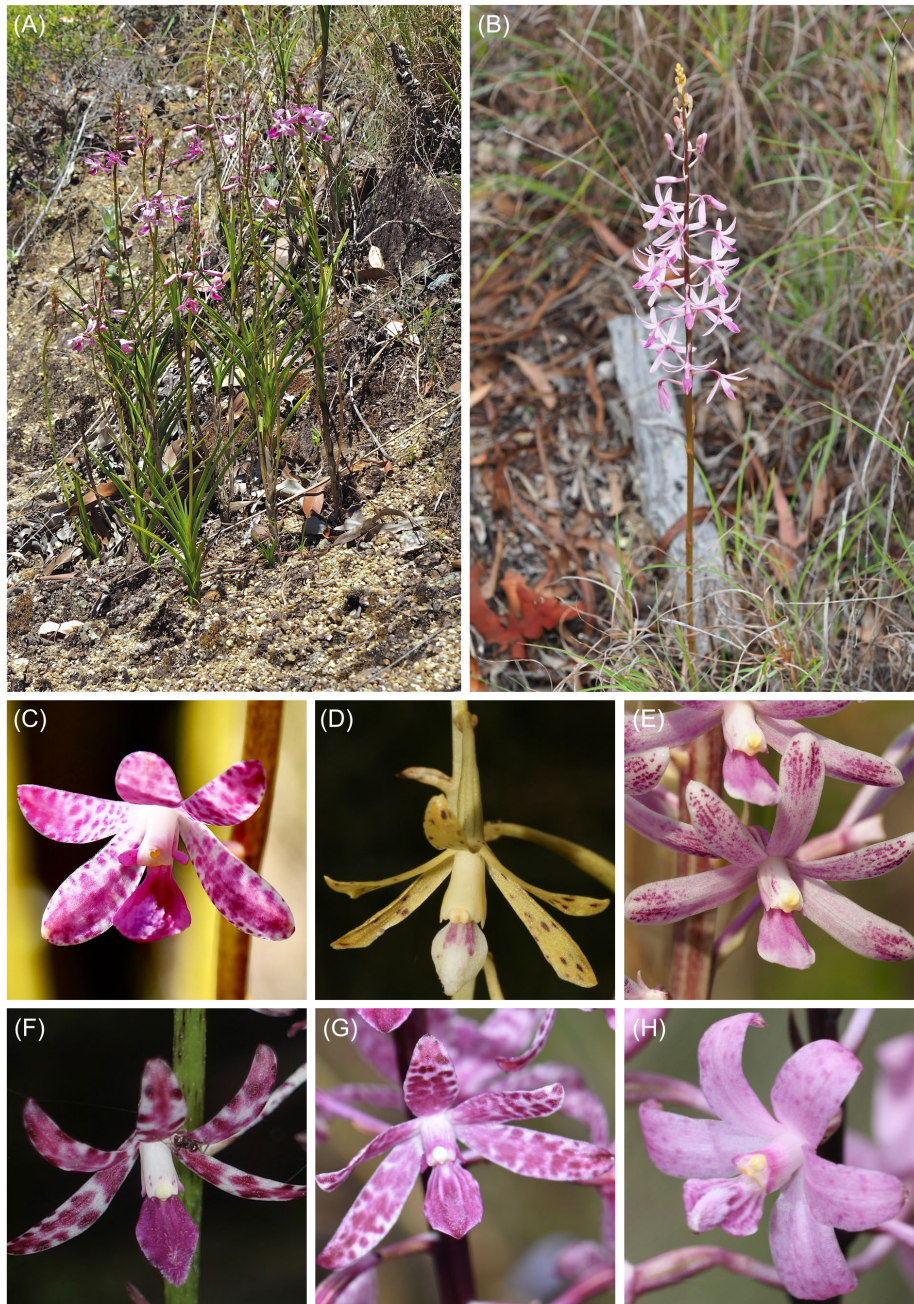
83 conceptual models to predict the evolutionary transition from autotrophy to heterotrophy of the  
84 plastid organelle (e.g., Graham et al., 2017; Barrett et al., 2019). Several studies in  
85 mycoheterotrophic orchid lineages found support for these models which predict a progression  
86 from losses of the chloroplast *ndh* genes to genes encoding complexes which are directly  
87 involved in photosynthesis (e.g., *psa*, *psb*) to more general ‘housekeeping’ genes (e.g., *accD*,  
88 *matK*) (Wicke and Naumann 2018; Barrett et al., 2018; Barrett et al., 2019; Kim et al., 2020;  
89 Kim et al., 2023).

90 Interestingly, degraded *ndh* genes were also found in some autotrophic orchids (e.g., Kim et  
91 al., 2015; Niu et al., 2017; Kim and Chase 2017; Lallemand et al., 2019; Kim et al., 2023). This  
92 appears curious, as the *ndh* genes encode proteins of the NADH dehydrogenase complex (NDH  
93 complex) which is assumed to play a role in cyclic electron flow and thus fine-tunes  
94 photosynthesis (Yamori et al., 2015; Peltier et al., 2016). Degradation of *ndh* genes is  
95 hypothesised to have led to additional structural changes of the plastome (Kim et al. 2015). In  
96 particular, *ndhF* gene loss was correlated with shifts in the position of the junction of the  
97 inverted repeat/small single copy (IR/SSC) region in Orchidaceae and other plants (Kim et al.,  
98 2015; Niu et al., 2017; Dong et al., 2018; Roma et al., 2018; Thode and Lohmann 2019; Li et  
99 al., 2021; Könyves et al., 2021). However, within Orchidaceae, degradation of *ndh* genes was  
100 found to vary even among closely related species (e.g., Kim et al., 2015; Feng et al., 2016; Kim  
101 and Chase, 2017; Barrett et al., 2018; Barrett et al., 2019) which suggests the genes for the  
102 NDH complex may be under relaxed selective pressure in several orchid lineages (Kim and  
103 Chase, 2017). Moreover, previous studies found that *ndh* degradation patterns vary  
104 considerably and have been independently degraded among orchids (Kim et al., 2015; Niu et  
105 al., 2017; Kim and Chase 2017; Lallemand et al., 2019).

106 The orchid genus *Dipodium* R.Br. (Cymbidieae) contains both autotrophic and  
107 mycoheterotrophic species and thus represents a suitable model system in which to address  
108 hypotheses of plastome evolution. The genus comprises 39 species and is divided into two  
109 sections, *Dipodium* and *Leopardanthus* (Blume) O. Kuntze, based on morphological and  
110 geographical evidence (O’Byrne, 2017; Jones, 2021). Sect. *Leopardanthus* (26 species) is  
111 distributed in the floristic regions of Malesia and Australasia (O’Byrne, 2017). All species of  
112 sect. *Leopardanthus* are green leafy plants and non-uniform in habit (O’Byrne, 2017). Section  
113 *Dipodium* occurs predominantly in Australasia, with nearly all species being endemic in  
114 Australia. One species occurs in New Guinea (*D. elatum* J.J.Sm.), one species extends into the  
115 Pacific region (*D. squamatum* (G.Forst.) Sm. (New Caledonia and Vanuatu), and one occurs  
116 in Malesia (*D. gracile* Schltr. (Sulawesi) (Schlechter, 1911; O’Byrne, 2017; POWO, 2023;

117 WFO, 2023). In contrast to sect. *Leopardanthus*, most species of sect. *Dipodium* are non-  
118 climbing terrestrials, forming subterranean rhizomes and erect flowering stems with highly  
119 reduced, non-photosynthetic leaves (i.e., scales) (**Figure 1, B**). Hence, species within sect.  
120 *Dipodium* are generally assumed to be fully mycoheterotrophic (O'Byrne, 2014). However,  
121 one Australian species of sect. *Dipodium*, *D. ensifolium* F.Muell., stands out as a leafy  
122 terrestrial (**Figure 1, A**).

123



124  
125  
126  
127  
128

**Figure 1:** Habit and flowers of *Dipodium* sect. *Dipodium*. A. *D. ensifolium*; B. *D. elegantulum* (note the green to purplish inflorescence stem); C. *D. ensifolium*; D. *D. interaneum*; E. *D. elegantulum*; F. *D. variegatum*; G. *D. punctatum*; H. *D. roseum*. (Photos: A-C, E: S. Goedderz; D, F -H: M.A. Clements.)

129 The aims of this study were to:

- 130 1. sequence and assemble plastid genomes for species of *Dipodium* to elucidate patterns of  
131 plastid genome modification (e.g., rearrangement, structural variation, pseudogenisation,  
132 gene loss) across autotrophs and mycoheterotrophs within the genus and examine gene  
133 degradation in context of current models of plastome degradation in heterotrophic plants.
- 134 2. infer phylogenomic relationships within section *Dipodium* and among closely related  
135 autotrophic relatives (i.e., *Dipodium* section *Leopardanthus*).
- 136 3. estimate divergence times of *Dipodium* to assess the origin of mycoheterotrophy within the  
137 genus and elucidate over which evolutionary timeframes plastid gene degradation and  
138 losses has taken place within *Dipodium*.

## 139 **2 Material and methods**

### 140 **2.1 Plant material**

141 For this study, we sampled all known Australian species of section *Dipodium* and one  
142 representative of section *Leopardanthus* (**Table 1**). Based on previous molecular systematic  
143 studies (Serna-Sánchez et al., 2021; Pérez-Escobar et al. 2023; Zhang et al. 2023), an extended  
144 outgroup from closely related orchid genera within subtribe Eulophiinae (*Eulophia* R.Br.,  
145 *Geodorum* Andrews) and subtribe Cymbidiinae (*Cymbidium* Sw., *Acriopsis* Reinw. ex. Blume)  
146 was sampled (**Table 1**). Specimens studied were from different regions within Australia, with  
147 the exception of one specimen from Papua New Guinea (*D. pandanum* 2) (**Table 1**).

### 148 **2.2 DNA extraction, library preparation, and sequencing**

149 Standard plant DNA extractions were carried out from 5-20 mg of silica dried plant tissue from  
150 field collections or herbarium material (**Table 1**) at the National Research Collections Australia  
151 (NRCA, CSIRO) in Canberra. The Invisorb DNA Plant HTS96 kit (Stratec, Birkenfeld,  
152 Germany) was used following the manufacturer's protocol, with a final elution of 60 ml.

153 DNA of *Dipodium* samples (**Table 1**) was sonicated to an average target length of ca. 200 bp  
154 using a LE220 sonicator (Covaris, Bankstown, Australia). After sonication, DNA length and  
155 concentration were quantified on Fragment Analyzer (Agilent Technologies, California, USA)  
156 using the Agilent high-sensitivity genomic DNA kit.

157 DNA libraries were prepared using the QiaSeq UltraLow Input library kit (Qiagen,  
158 Germantown, Australia) using custom dual-indexed adapters. Final libraries were size-selected  
159 on Fragment Analyzer using the high-sensitivity Genomic Fragment Analyzer Kit (Agilent,  
160 Santa Clara, USA), quantified using the Fluoroskan plate fluorometer (Thermo Fisher

161 Massachusetts, USA) and the Quant-iT HS dsDNA kit (Invitrogen, California, USA) following  
162 the manufacturer's instructions. Samples were pooled equimolarly and sequenced using 150  
163 bp paired end reads on a NovaSeq S1 flowcell (Illumina, California, USA) at the Biomolecular  
164 Resource Facility within the John Curtin School of Medical Research, Australian National  
165 University (Canberra, Australia).

### 166 **2.3 Data processing and whole plastid genome assembly**

167 We carried out both *de novo* and reference-guided assemblies for the *Dipodium* data set.  
168 Trimming and assembly of *de novo* contigs were carried out as described in Nargar et al.  
169 (2022). Briefly, raw sequences were trimmed applying a Phred score > 20 using Trimmomatic  
170 0.39 (Bolger et al., 2014), and deduplicated using 'clumpify' from BBtools 38.9 (Bushnell,  
171 2014). Read pairs were then assembled using SPAdes 3.15 (Bankevich et al., 2012). Plastid  
172 databases were extracted from NCBI's Nucleotide Entrez database using Entrez Programming  
173 Utilities (2008) using taxonomic, keyword, and sequence length constraints. Contigs were  
174 identified as derived from plastid source using blastn against these databases. Genes within  
175 plastid contigs were identified by homology using BLAST (Altschul et al., 1990) and BLASTx  
176 (RRID:SCR\_001653) against genes extracted from annotations of the reference sequence sets  
177 extracted from nuccore.

178 Reference-guided assemblies were performed with paired, merged reads and the recently  
179 published and closely related plastome of *Dipodium roseum* D.L.Jones and M.A.Clem.  
180 (MN200386, Kim et al., 2020). The related orchid *Masdevallia coccinea* Linden ex Lindl.  
181 (KP205432, Kim et al., 2015) was included as an additional reference sequence to ensure that  
182 regions which already showed degradation in some plastid genes in the plastome of *D. roseum*  
183 (e.g., all *ndh* genes) (MN200386, Kim et al., 2020) and which may still be present in other  
184 *Dipodium* species could be assembled as the plastome of *M. coccinea* has a full set of functional  
185 plastid genes (Kim et al., 2015).

186 Reference-guided assemblies were carried out using the plugin 'map to reference' in Geneious  
187 Prime (Version 2022.0.2, Biomatters Ltd, [www.geneious.com](http://www.geneious.com)) with default settings. To obtain  
188 complete plastome assemblies, consensus sequences for each sample were extracted (threshold  
189 60%, reading depth > 10), aligned using MAFFT v7.388 (Katoh and Standley 2013) in  
190 Geneious, manually checked and compared. Reference-guided assemblies were visually  
191 inspected and in cases of misassembled regions due to potential mismatches between the  
192 sample and the reference *de novo* assemblies were consulted, and were quality allowed the  
193 region extracted from the *de novo* assembly. The prediction and finding of gene annotations

194 for complete plastome assemblies were performed with the Geneious plugin ‘predict  
195 annotation’ (similarity: 90% and best match with *D. roseum* (MN200386)). Open reading  
196 frames (ORFs) were manually checked and verified by identifying the start and stop codons.  
197 In cases of remaining ambiguities, BLAST searches were conducted for reading-frame  
198 verification (Altschul et al. 1990; National Center for Biotechnology Information; Available  
199 from: <https://blast.ncbi.nlm.nih.gov/Blast.cgi> [cited: 08 Sept 2023]). The inverted repeat (IR)  
200 boundaries were identified using the ‘repeat finder’ plugin in Geneious with default settings.  
201 In total, 24 complete *Dipodium* plastomes were assembled in this study. The graphical  
202 representation of each plastome and divergent regions with annotations were created in  
203 OrganellarGenomeDRAW (OGDRAW, version 1.3.1, Greiner et al., 2019).

#### 204 **2.4 Phylogenetic analyses**

205 To elucidate phylogenetic relationships within *Dipodium* and to assess the phylogenetic  
206 position of *Dipodium* within Cymbidieae we performed a phylogenetic analysis with DNA  
207 sequences of 33 newly sequenced plastomes from this study (**Table 1**) and an extended  
208 outgroup sampling for 115 samples from published plastid data (Supplementary Material 1).

209 Coding regions of respective genes of 33 samples were extracted with the ‘extract’ function in  
210 Geneious Prime. Where mutations had led to frame shifts with internal stop codons, the  
211 affected sequences were excluded from phylogenetic analyses.

212 Each extracted coding region of in total 68 plastid loci from 33 samples (including the intron  
213 regions) and from 115 published plastomes (excluding intron regions) were aligned using  
214 MAFFT (v7.388; Katoh et al., 2002; Katoh and Standley 2013) Geneious prime plugin with  
215 default settings, checked manually and subsequently concatenated to an alignment of 69,335  
216 bp (Supplementary Material 2).

217 Maximum likelihood analysis of the plastid dataset (148 samples) with best-fit models  
218 GTR+I+I+F+R4 was performed using IQ-TREE ver. 2.2.0 (Nguyen et al., 2015;  
219 Kalyaanamoorthy et al., 2017; Minh et al., 2020). Branch support was obtained with  
220 Shimodaira-Hasegawa-like approximate Likelihood Ratio Test (SH-aLRT; Guindon et al.,  
221 2010) and the ultrafast bootstrap (ufboot2; Hoang et al., 2018) as implemented in the IQ-TREE  
222 software. The tree topology was visualised using the software Figtree (ver. 1.4.4.;;  
223 <http://tree.bio.ed.ac.uk/software/figtree/>).

224

225



## 226 2.5 Divergence-time analysis

227 For divergence-time estimations of *Dipodium*, the alignments were reduced to the 30 most  
228 parsimony informative loci due to computational limitations. The 30 plastid loci were selected  
229 based on their most parsimony informative (Pi) sites estimated with MEGA (Molecular  
230 Evolutionary genetics Analysis; ver. 11.0.11, Tamura et al., 2021) and presence of loci across  
231 the dataset (Supplementary Material 2). For taxa represented by more than one sample,  
232 duplicates were removed from alignments as recommended for divergence time estimation.  
233 Alignments of 30 plastid loci from 134 taxa were concatenated yielding a total alignment length  
234 of 27,934 bp using MAFFT (v7.388; Katoh et al., 2002; Katoh and Standley 2013)  
235 implemented in Geneious Prime (Supplementary Material 2). Absolute node ages and  
236 phylogenetic relationships were jointly estimated in BEAST (ver. 2.7.4; Bouckaert et al., 2019,  
237 Bouckaert et al. 2014) applying the best fit partition scheme and substitution model as  
238 determined by IQ-TREE's ModelFinder (GTR+F+I+R4). Four different models were tested:  
239 a Bayesian optimised relaxed and a strict molecular clock with uncorrelated lognormal rates  
240 with each a Yule and a Birth-death tree prior on the speciation process (Douglas et al., 2021;  
241 Gernhard et al., 2008; Zuckerkandl and Pauling, 1965; Yule, 1925). Trees were calibrated with  
242 four secondary calibration points based on Zhang et al. (2023). A normal distribution with an  
243 offset value of 101.52 Ma and a standard deviation (SD) of 2.2 was assigned as crown age of  
244 Orchidaceae. The priors for the three other calibration points were set with a normal  
245 distribution and the means of stem ages for Vanilloideae (offset value = 93.48 Ma, SD = 2.7),  
246 Cyripedioideae (offset value = 89.14 Ma, SD = 2.71) and Orchidoideae (offset value = 77.74  
247 Ma, SD = 2.0). For each clock model, 10 parallel BEAST analyses with each 30 million  
248 generations and a sampling frequency of every 10,000 generations were carried out. The run  
249 parameters were examined in TRACER (ver. 1.7.2; Rambaut et al., 2018) and the effective  
250 sample sizes (ESSs) of > 200 for all parameters and the burn-in were assessed. The runs were  
251 combined in LogCombiner (Drummond and Rambaut 2007) with a burn-in of 10% and  
252 subsequently used to generate a maximum-clade-credibility chronogram with mean node  
253 heights in TreeAnnotator (Drummond and Rambaut 2007). To determine the best fitting clock  
254 model and speciation models for the data set, a model comparison using the AICM (Akaike  
255 Information Criterion by MCMC) was performed with BEAST v.2.6.2 and evaluated with the  
256 AIC model selection criterion of Fabozzi et al. (2014).

257

258

## 259 2.6 Plastid genome evolution

### 260 2.6.1 Structural variation in *Dipodium* plastomes

261 To examine structural variation among the plastomes of *Dipodium*, whole plastome alignments  
262 were generated using MAFFT (v7.388; Katoh et al., 2002; Katoh and Standley 2013)  
263 implemented in Geneious Prime with full annotations. Alignments were manually checked, in  
264 cases of divergent regions e.g., the operon region of *ndhC*, *ndhK*, and *ndhJ* genes or junctions  
265 between the large single copy (LSC)/ inverted repeat B (IRB)/ small single copy (SSC)/  
266 inverted repeat A (IRA) regions, and respective regions (including annotations) were extracted  
267 in Geneious Prime, separately aligned, proofread, and subsequently visualised using  
268 OGDRAW (ver. 1.3.1, Greiner et al., 2019).

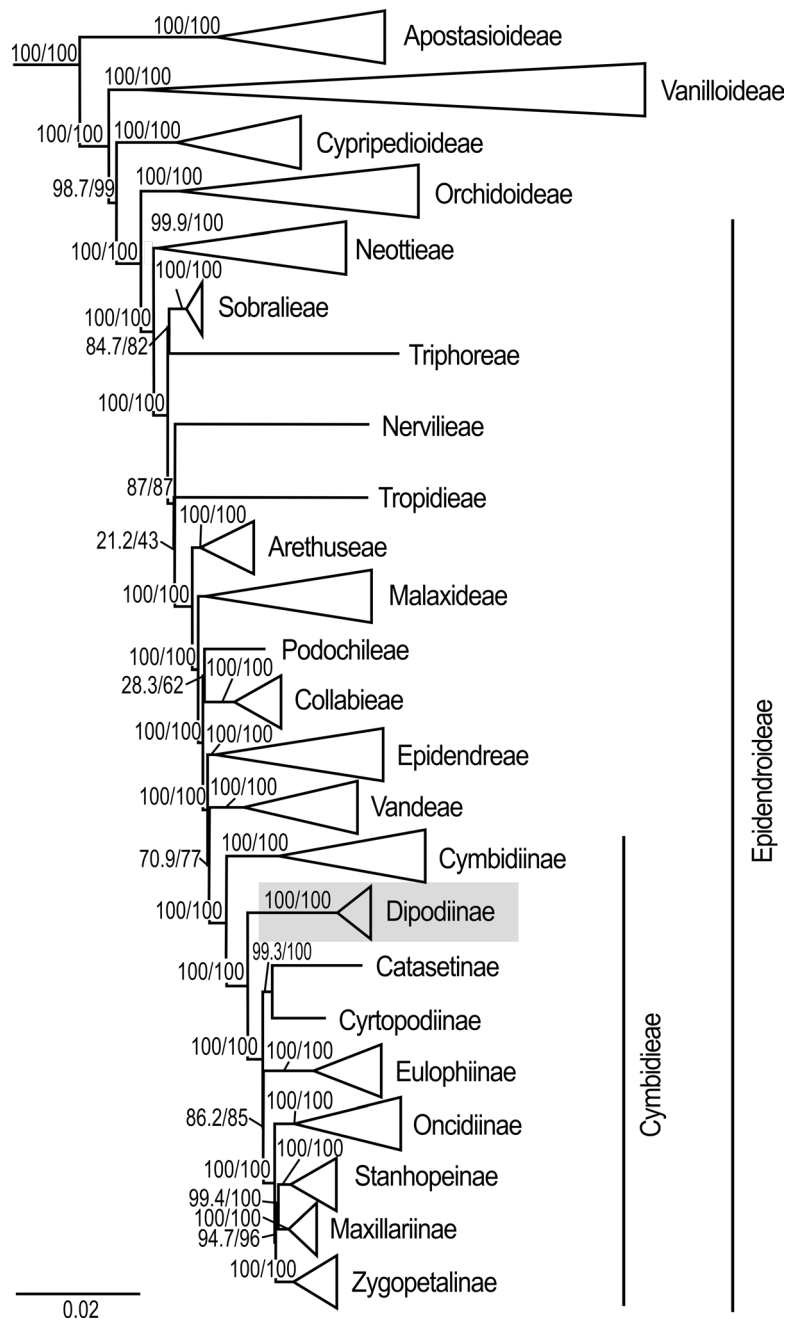
### 269 2.6.2 Functional genes, pseudogenes, and physical gene loss

270 To classify the level of degradation of plastid genes in *Dipodium*, we used the following  
271 categories: (1) **functional** - the reading frame was intact and less than 10% of the open reading  
272 frame was disrupted by small indels; (2) **moderately pseudogenised** - less than 10% of the open  
273 reading frame was disrupted by internal stop codons or indels causing non-triplet frame shifts;  
274 (3) **severely pseudogenised** - more than 10% of the open reading frame was disrupted by either  
275 internal stop codons, large deletions (> 10%), and non-triplet frame shifts (based on Barrett et  
276 al., 2019), or (4) **lost** - the gene was not identified in the annotation process of the *de-novo*  
277 assembly (e.g., Joyce et al., 2018) and/or was not detectable within the reference-guided  
278 assembly. A gene was considered as not detectable within the reference-guided mapping  
279 process if at least 70% of the gene sequence could not be identified for calculation of the  
280 consensus sequence within the Geneious mapping process. The coded matrix of gene  
281 degradation was plotted against the maximum likelihood phylogenetic tree of *Dipodium*.

## 282 3 Results

### 283 3.1 Phylogenetic placement of *Dipodium* in tribe Cymbidieae and infrageneric 284 relationships within the genus

285 The maximum likelihood analysis based on 68 plastid loci and 148 samples yielded highly  
286 resolved and well-supported tree topologies for the phylogenomic relationships within  
287 Orchidaceae (Supplementary Material 3). Within Epidendroideae, Cymbidiinae was  
288 monophyletic and sister to all other Cymbidieae including Dipodiinae (SH-aLRT/UFboot  
289 100/100; **Figure 2**). *Dipodium* was retrieved as next diverging lineage within Cymbidieae and  
290 monophyletic with maximum support values (SH-aLRT/UFboot 100/100; **Figure 2**).



291

292 **Figure 2:** Phylogenetic relationships among major orchid lineages and placement of subtribe  
 293 *Dipodiinae* in Cymbidieae. Maximum likelihood tree of 148 taxa based on 68 plastid loci. Support  
 294 values are shown above each branch, SHaLRT followed by UFboot values. Scale bar represents branch  
 295 length, along which 0.02 per-site substitutions are expected. Detailed phylogeny provided in  
 296 Supplementary Material 3.

297

298 Within *Dipodium*, section *Leopardanthus* was placed as sister group to section *Dipodium* with  
 299 maximum support values (SH-aLRT/UFboot 100/100; **Figure 3**).

300 Section *Dipodium* was resolved as monophyletic and divided into six highly supported  
 301 lineages. The leafy species *D. ensifolium* was placed as sister to all leafless species of the  
 302 section (SH-aLRT/UFboot 100/100; **Figure 3**). Next, sect. *Dipodium* split into two main

303 clades, A and B (SH-aLRT/UFboot 99/100; **Figure 3**). Clade A split into two lineages, the  
 304 *Dipodium hamiltonianum* complex and the *Dipodium stenocheilum* complex, receiving  
 305 maximum nodal support (SH-aLRT/UFboot 100/100; **Figure 3**). The *D. hamiltonianum*  
 306 complex comprised the two species *D. hamiltonianum* and *D. interaneum*. The *D. stenocheilum*  
 307 complex included *D. ammolithum*, *D. basalticum*, *D. elegantulum*, *D. stenocheilum*, and *D. aff.*  
 308 *stenocheilum*. *Dipodium stenocheilum* was retrieved as non-monophyletic. (**Figure 3**).

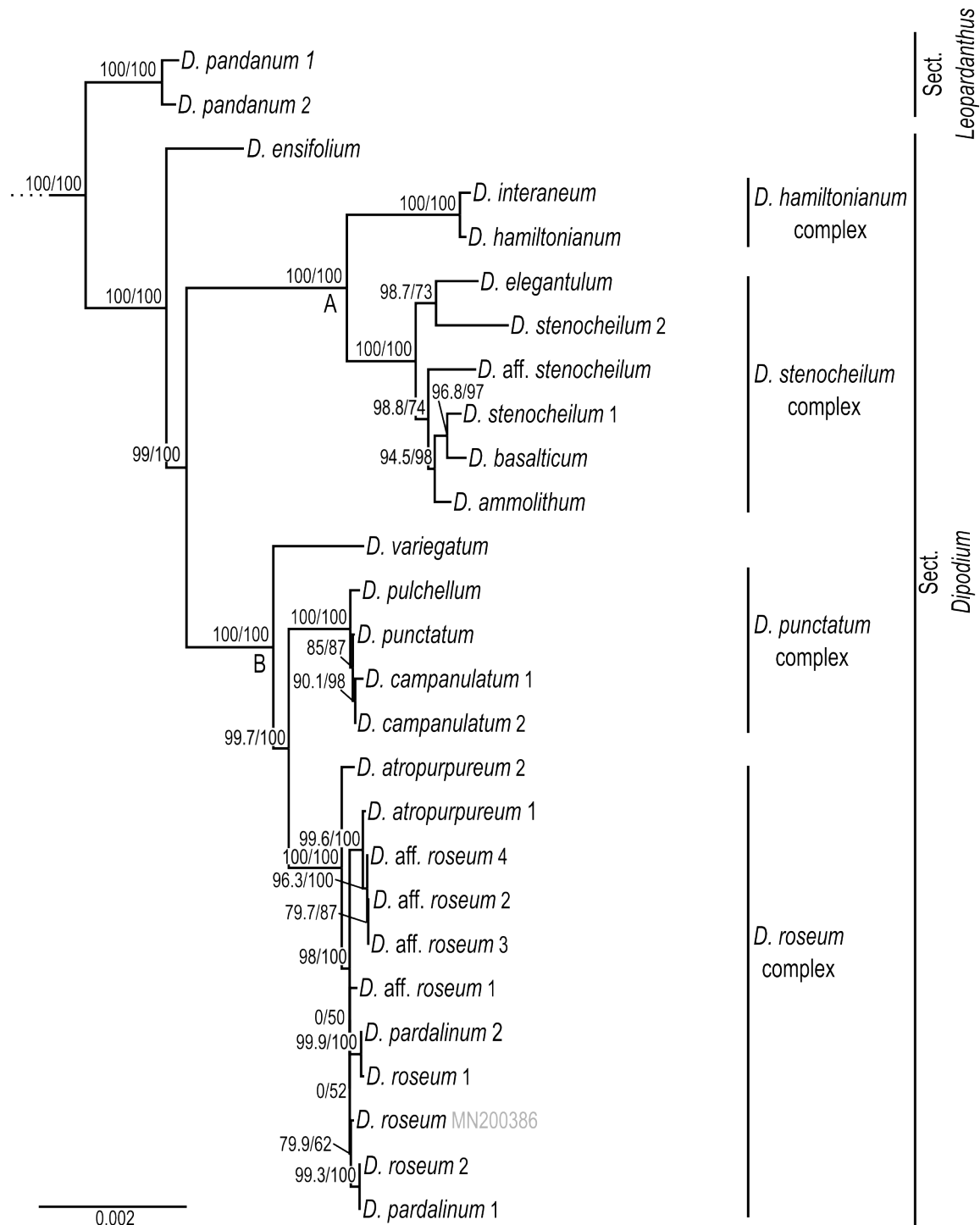


**Figure 3:** Phylogenetic relationships in *Dipodium*. Maximum likelihood tree based on 68 plastid loci and 148 taxa (outgroups not shown). Support values are given above each branch, SHaLRT is followed

312 by UFBoot values. Scale bar represents branch length, along which 0.002 per-site substitutions are  
313 expected.

314

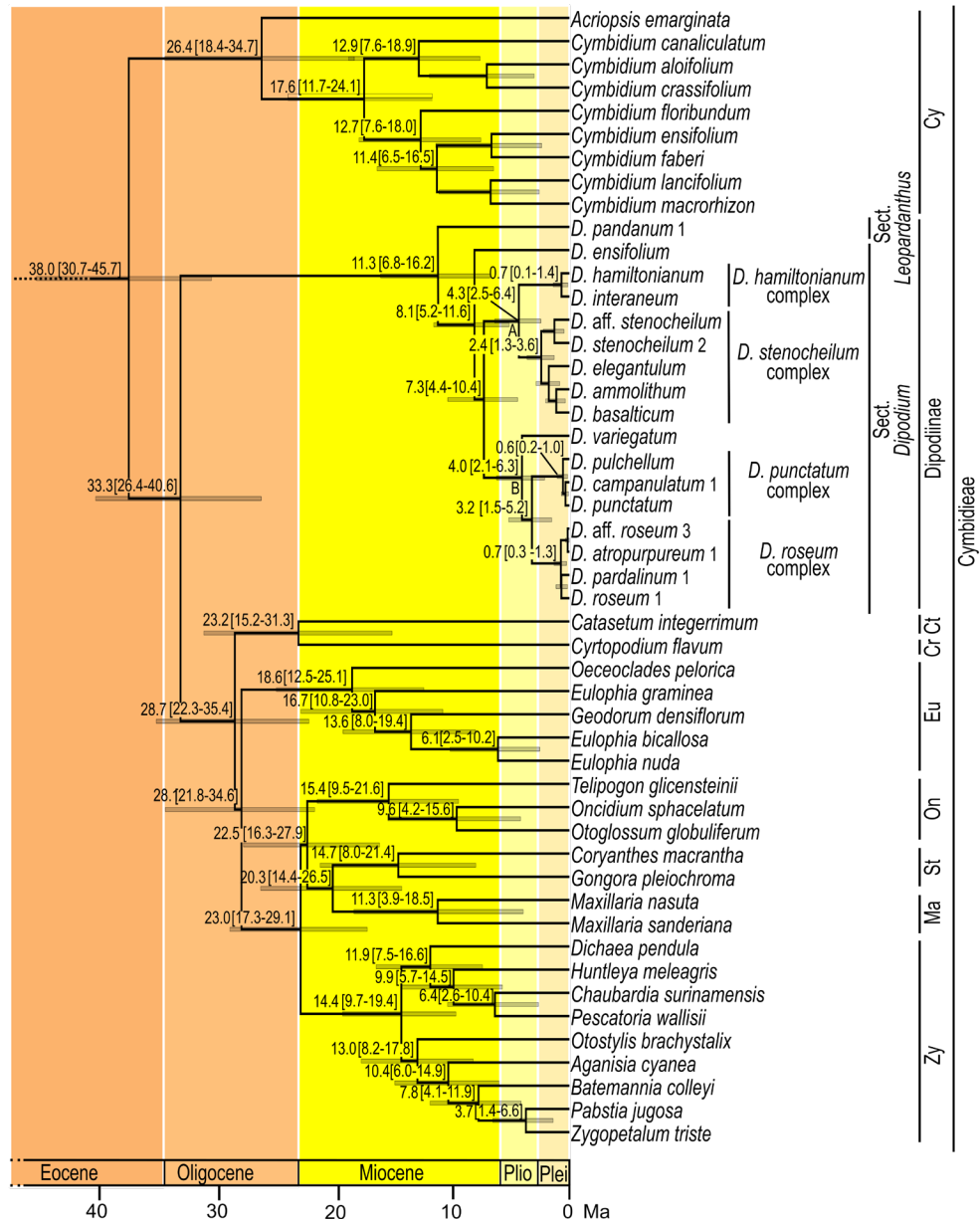
315 Clade B resolved *D. variegatum* as sister to the remaining species of the clade (SH-  
316 aLRT/UFboot 100/100). The remainder split into the *D. punctatum* complex and the *D. roseum*  
317 complex (SH-aLRT/UFboot 99.7/100; **Figure 3**). The *D. punctatum* complex comprised three  
318 species, *D. campanulatum*, *D. pulchellum*, and *D. punctatum*. Phylogenetic divergence  
319 between these three species was shallow and support for interspecific relationships within the  
320 complex low. The *D. roseum* complex comprised four taxa, namely *D. atropurpureum*, *D.*  
321 *pardalinum*, *D. roseum*, and *D. aff. roseum*. Resolution and support for interspecific  
322 relationships within the *D. roseum* complex was low overall.

### 323 **3.2 Divergence-time estimations**

324 Absolute times of divergence under strict and optimised relaxed clocks for Orchidaceae based  
325 on 30 plastid loci and 134 taxa showed similar results. Strict clock models consistently yielded  
326 slightly older age estimates than the analyses based on the relaxed clock models  
327 (Supplementary Material 4). Model comparison using AICM (Fabozzi et al., 2014) identified  
328 the relaxed clock model under the birth-death speciation model as the best fit models for the  
329 dataset (Supplementary Material 4).

330 The Bayesian relaxed clock tree topology and the maximum likelihood phylogeny agreed  
331 overall in major relationships within Orchidaceae and the placement of species within  
332 *Dipodium*. Epidendroideae were estimated to have emerged ca. 77.7 Ma (HDP: 74.2–81.5)  
333 with the stem age of subtribe Cymbidieae placed in the Eocene, ca. 42.2 Ma (HDP: 34.3–50.1)  
334 (Supplementary Material 4 and 5). The stem age of subtribe Cymbidiinae, the first diverging  
335 lineage in Cymbidieae, was placed in the late Eocene, ca. 38.0 Ma (HDP: 30.7–45.7) (**Figure**  
336 **4**). Stem diversification of Dipodiinae was estimated to have commenced ca. 33.3 Ma (HDP:  
337 26.4–40.6) in the early Oligocene (**Figure 4**). Crown diversification of Dipodiinae was  
338 estimated to have commenced much later, in the late Miocene with sections *Dipodium* and  
339 *Leopardanthus* diverging ca. 11.3 Ma (HDP: 6.8–16.2) (**Figure 4**). The crown age of section  
340 *Dipodium* was estimated to be ca. 8.1 Ma (HDP: 5.2–11.6) in the late Miocene with the  
341 divergence of the leafy species, *D. ensifolium*, from the remainder of section *Dipodium* (**Figure**  
342 **4**). The crown age of the remainder of the section, i.e., all leafless species, was estimated to ca.  
343 7.3 Ma (HDP: 4.4–10.4) (**Figure 4**). Within this leafless clade, two subclades each containing  
344 two species complexes were resolved. The crown age of the clade comprising the *D.*  
345 *hamiltonianum* complex and the *D. stenocheilum* complex was estimated to ca. 4.3 Ma

346 (HDP:2.5–6.4) in the early Pliocene (**Figure 4**) which is congruent with estimations of the  
 347 crown age of clade B (comprising *D. variegatum* and the two complexes *D. punctatum* and *D.*  
 348 *roseum*) (**Figure 4**). The *D. stenocheilum* complex had a crown age of ca. 2.4 Ma (HDP: 1.3–  
 349 3.6) in the early Pleistocene. The three remaining complexes had crown ages estimated to the  
 350 mid Pleistocene (*D. hamiltonianum* complex: ca. 0.7 Ma, HDP: 0.1–1.4; *D. punctatum*  
 351 *complex*: ca. 0.6 Ma, HDP: 0.2–1.0, and *D. roseum* complex: ca. 0.7 Ma, HDP: 0.3–1.3)  
 352 (**Figure 4**).



353  
 354 **Figure 4:** Chronogram of Cymbidiaceae. Maximum-clade-credibility tree from Bayesian divergence-time  
 355 estimation in BEAST2 based on 30 plastid loci and an optimised lognormal molecular clock model  
 356 under the birth-death prior (outgroups not shown). Divergence times (million years ago) are shown at  
 357 each node, together with 95% highest posterior density (HDP) values indicated by grey bars and values  
 358 in parentheses. A and B refers to the two main lineages within sect. *Dipodium*. Cy: Cymbidiinae, Ct:  
 359 Catasetinae, Cr: Cyrtopodiinae, Eu: Eulophiinae, On: Oncidiinae, St: Stanhopeinae, Ma: Maxillariinae,

360 Zy: Zygotetaliae, Plio: Pliocene, Plei: Pleistocene. Outgroups to Cymbidieae not shown. Detailed  
361 chronogram provided in Supplementary Material 5.

### 362 **3.3 Characterisation of *Dipodium* plastomes**

363 Complete plastome assemblies and annotations were successfully carried out for 24 *Dipodium*  
364 samples, representing all Australian species of section *Dipodium* including two recently  
365 discovered species of section *Dipodium* (*D. ammolithum* and *D. basalticum*), two putatively  
366 new species of section *Dipodium* (*D. aff. roseum*, *D. aff. stenocheilum*) and one species of  
367 section *Leopardanthus* (*D. pandanum*) (**Table 2**). Plastome assemblies for *D. pandanum* 2 and  
368 *D. aff. stenocheilum* showed an insufficient mean coverage (<30) for non-coding regions which  
369 caused unsolved gaps and ambiguous bases which could not be reliably resolved. The number  
370 of paired-end, trimmed reads for the successfully assembled complete plastomes ranged from  
371 332,604 (*D. pandanum* 1) to 27,999,734 (*D. pardalinum* 2) and the mean coverage ranged from  
372 31x to 627x (Supplementary Material 6).

#### 373 **3.3.1 Plastome features and structural variations within *Dipodium* plastomes**

374 Plastome sizes of *Dipodium* ranged from 142,949 bp (*D. variegatum*) to 152,956 bp (*D. aff.*  
375 *roseum* 3) (**Table 2, Figure 5**, Supplementary Material 7). The largest average plastome size  
376 (150,578 bp) was found in the *D. roseum* complex, closely followed by the leafy *D. ensifolium*  
377 (150,084 bp), and the *D. punctatum* complex (149,512 bp). Plastome sizes within the *D.*  
378 *stenocheilum* complex were markedly lower with an average size of 146,305 bp. Similarly  
379 small plastomes were also found in *D. hamiltonianum* (145,902 bp), *D. interaneum* (146,497  
380 bp) and the leafy climber *D. pandanum* 1 (sect. *Leopardanthus*) (146,204 bp) (**Table 2**).  
381 *Dipodium* plastomes possess the typical quadripartite structure of angiosperms, with the SSC  
382 region ranging from 12,039 bp (*D. variegatum*) to 16,756 bp (*D. ensifolium*), the LSC region  
383 ranging from 81,514 bp (*D. stenocheilum* 2) to 83,172 bp (*D. punctatum*), and the pair of IRs  
384 ranging from 24,436 bp (*D. variegatum*) to 26,817 bp (*D. aff. roseum* 3) (**Table 2**).

385 Total mean GC content of *Dipodium* plastomes was 36.9%, ranging between 36.8% (*D. roseum*  
386 2 and *D. pardalinum* 1) and 37.1% (*D. hamiltonianum*) (**Table 2**). Within the *D. roseum*  
387 complex the GC content was 36.8% – 36.9%, followed by the *D. punctatum* complex (36.9%),  
388 *D. stenocheilum* complex (37.0%) and the highest GC content was 37.1% and 37.0% (*D.*  
389 *hamiltonianum* and *D. interaneum*) (**Table 2**).

390 The plastid genes of each plastome were rated as functional; moderately to severely  
391 pseudogenised; or physically lost. The total number of functional genes in *Dipodium* plastomes  
392 ranged slightly from 119 to 121 including a total of 73 or 74 functional protein-coding sequence

393 regions (CDS) (68 or 69 unique CDS), 37 to 39 functional tRNA genes (30 or 31 unique tRNA  
394 genes) and 8 rRNA genes (4 unique rRNA genes) (**Table 2**).

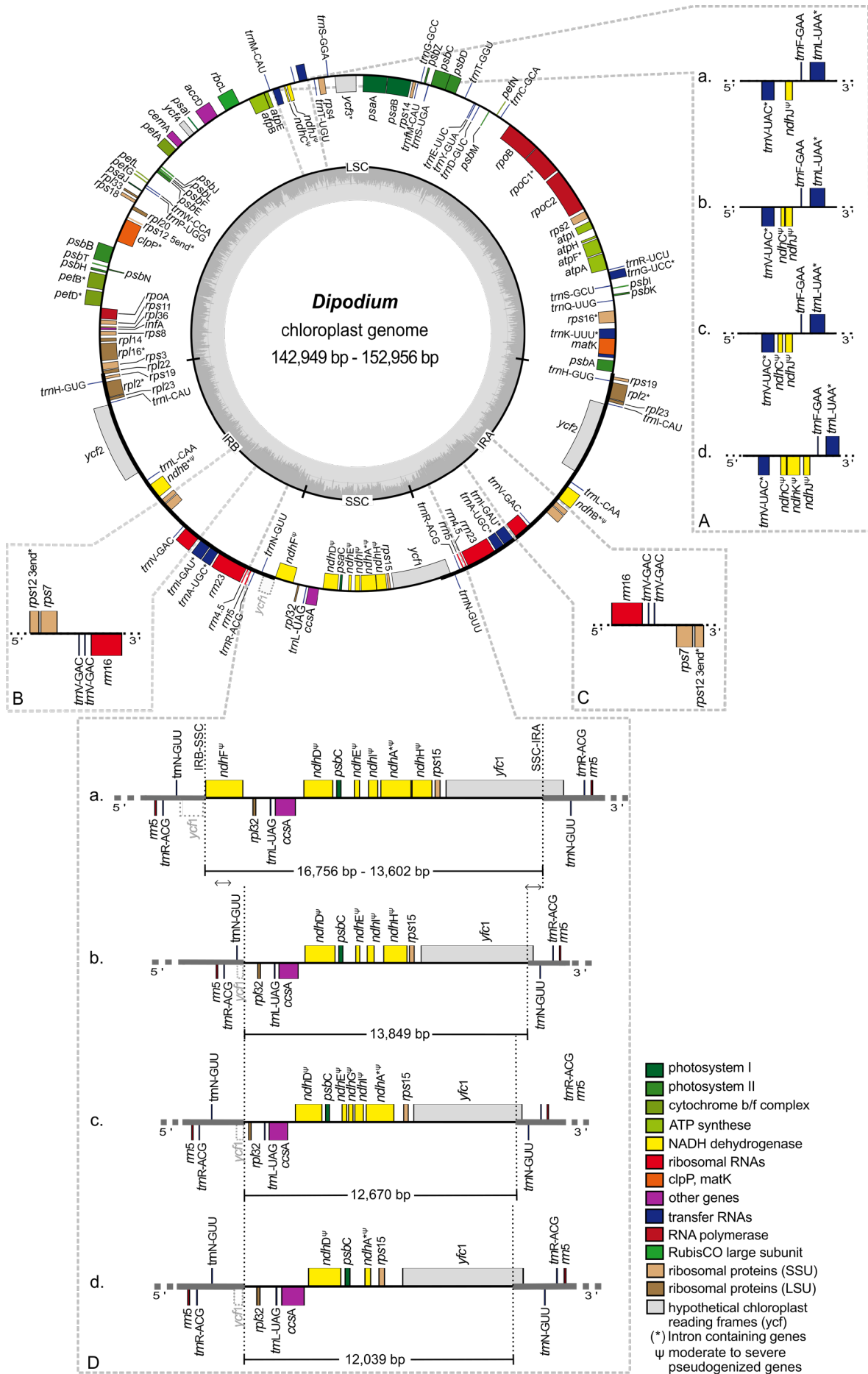
395 The IR region was largely conserved among all examined *Dipodium* plastomes. All species  
396 showed six duplicated coding regions in the IRs (i.e., *rpl2*, *rpl23*, *rps7*, *rps12*, *rps19*, *ycf2*) and  
397 all four rRNA genes (**Table 3**). Most plastomes showed eight duplicated tRNA genes in the IR  
398 regions with exception of the plastomes of *D. interaneum* and *D. elegantulum* which comprised  
399 a duplicated *trnV*-GAC within the IRB and the plastomes of *D. ammolithum*, *D.*  
400 *hamiltonianum*, and *D. stenocheilum* 2 which contained a duplicated *trnV*-GAC within the IRA  
401 (**Table 3, Figure 5, B & C**). All plastomes contained 16 functional intron-genes (i.e., *atpF*,  
402 *clpP*, *petB*, *petD*, *rpl2*, *rpl16*, *rpoC1*, *rps12*, *rps16*, *trnA*-UGC, *trnG*-UCC, *trnI*-GAU, *trnK*-  
403 UUU, *trnL*-UAA, *trnV*-UAC, *ycf3*), except for *D. pandanum* 1 which possessed two  
404 pseudogenes with introns (i.e., *ndhA*, *ndhB*) (**Table 3, Figure 5**). The *rps12* gene was trans-  
405 spliced with the 5' end located in the LSC region and 3' end was duplicated in the IRs in all  
406 studied plastomes (**Figure 5, Supplementary Material 7**).

407 The SSC region was found to vary the most among the examined samples. All plastomes  
408 showed a contraction of the SSC with a reduction of 20-40% compared to the average size of  
409 the angiosperm SSC regions (ca. 20 kb) (Ruhlman and Jansen 2014).

410 Three plastomes (*D. pandanum* 1, *D. stenocheilum* 1, *D. variegatum*) lost the *ndhF* gene. This  
411 complete loss of the *ndhF* gene resulted in the *ycf1* fragment being located in the vicinity of  
412 the *rpl32* (**Figure 5, D, b-d**) and caused a boundary shift of the IRB/SSC region located at the  
413 3' end of the *ycf1* fragment and spacer region of *rpl32* (**Figure 5**). While all other plastomes  
414 exhibited a severely truncated *ndhF* gene but did not exhibit an IRB/ SSC boundary shift  
415 (**Figure 5, Supplementary Material 7**). The IRA/SSC junction in all examined plastomes was  
416 located within the 5' portion of the functional *ycf1* gene, ranging from 97 bp (*D. pandanum* 1)  
417 to 1,072 bp (*D. aff. roseum* 3) (**Figure 5**).

418 In contrast to the instability of the IR/SSC boundaries, IR/LSC boundaries were found to be  
419 relatively stable. For all studied plastomes, the LSC/IRA boundaries were located near the 3'  
420 end of *psbA* (**Figure 5**). Variations within the LSC regions were limited to the operon which  
421 contained *ndhC*, J, K (**Figure 5, A**) and the independent pseudogenisation of *cemA* in the  
422 plastome of *D. aff. roseum* 4 and *trnD*-GUC in the plastome of *D. campanulatum* (**Table 3,**  
423 **Supplementary Material 7**).





425 **Figure 5:** Plastome map and boundary shifts in *Dipodium*. The plastome of *D. atropurpureum* 2 is  
426 illustrated as representative and shown as a circular gene map with the smallest and the largest  
427 *Dipodium* plastome of this study. Genes outside the circle are transcribed in a clockwise direction, those  
428 inside the circle are transcribed in a counterclockwise direction. The dark grey inner circle corresponds  
429 to the G/C content, and the lighter grey to the A/C content. The major distinct regions of complete  
430 *Dipodium* plastomes are compared in each detailed enlarged box (A-D). (A) Note that each  
431 representative block (a-d) has pseudogenised or lost either *ndhJ*, *ndhK* or *ndhC* genes. (B, C).  
432 Duplication of *trnV*-GAC in the Inverted Repeat regions of *D. interaneum* (IRB), *D. hamiltonianum*  
433 (IRA), *D. elegantulum* (IRB), *D. stenocheilum* 2 (IRA), *D. ammolithum* (IRA). (D) Each block (a. as  
434 representative *D. roseum* 2; b. *D. pandanum* 1; c. *D. stenocheilum* 1; d. *D. variegatum*) shows  
435 differences in the length (bp) of the SSC region caused through loss or pseudogenization of either *ndhF*,  
436 *ndhD*, *ndhE*, *ndhG*, *ndhI*, *ndhA* or *ndhH*, note the boundary shift of the IRs/SSC region caused through  
437 the loss/ pseudogenisation of *ndhF* and the inclusion of the functional *ycf1* and the *ycf1*-fragment (grey,  
438 dashed line) into the IRs. SSC: Small Single Copy; LSC: Large Single Copy; IRA/B: Inverted Repeat  
439 A/B.  
440

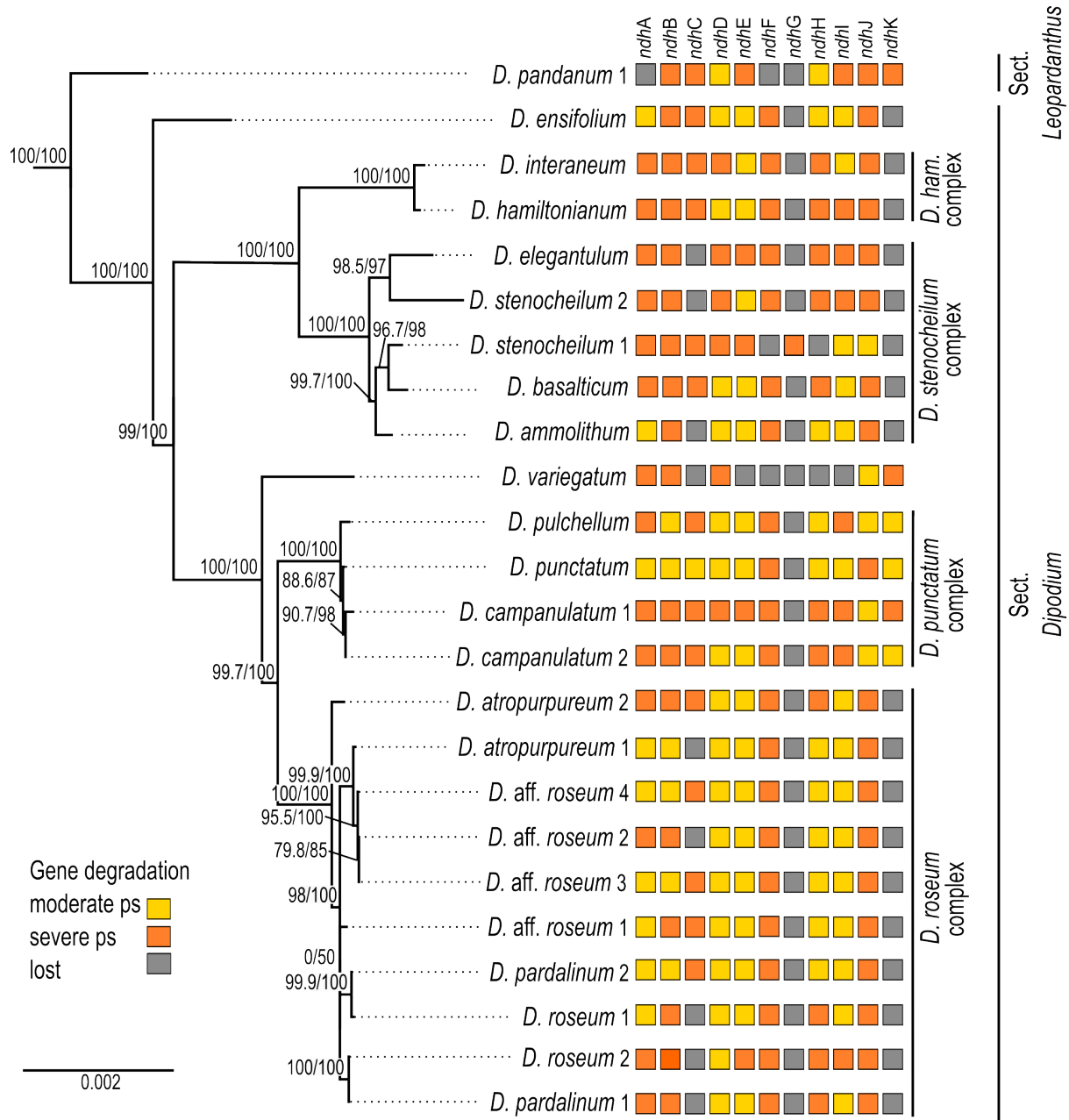
### 441 3.3.2 *ndh* gene degradation and loss in *Dipodium*

442 All *ndh* genes exhibited varying degrees of putative loss or pseudogenisation; not a single *ndh*  
443 gene remained functional in the examined *Dipodium* plastomes (Table 3, Figure 5 & 6).

444 The most severe *ndh* gene loss occurred in the plastome of *D. variegatum*, with *ndhA*, *ndhB*,  
445 *ndhD* and *ndhK* severely pseudogenised and *ndhJ* moderately pseudogenised.

446 The greatest degradation processes within *Dipodium* occurred for the *ndhG* gene, which was  
447 putatively lost in almost all plastomes, except *D. stenocheilum* 1 which retained a severely  
448 pseudogenised *ndhG* gene (Figure 6). This was followed by *ndhK*, which was lost in 19 out of  
449 24 plastomes (*D. ensifolium*, *D. hamiltonianum*, *D. interaneum*, the *D. roseum* complex and  
450 the *D. stenocheilum* complex) (Figure 6). In the six remaining plastomes *ndhK* was conserved  
451 to different degrees. *D. punctatum*, *D. pulchellum* and *D. campanulatum* 2 retained more than  
452 90% of the homologous bases compared to the functional *ndhK* gene of *M. coccinea*  
453 (KP205432, Kim et al., 2015) but showed severe frameshift mutations and indels which caused  
454 several internal stop codons. The plastomes with severely pseudogenised *ndhK* genes exhibited  
455 large truncations.

456 Nine *Dipodium* samples (*D. ammolithum*, *D. atropurpureum* 1, *D. elegantulum*, *D. pardalinum*  
457 1, *D. roseum* 1 & 2, *D. aff. roseum* 2, *D. stenocheilum* 2, and *D. variegatum*) putatively lost  
458 the *ndhC* gene. In *D. punctatum* *ndhC* was moderately pseudogenised and in the remaining  
459 plastomes *ndhC* was severely pseudogenised (Figure 6). Only *D. ensifolium* showed an intact  
460 start codon for the *ndhC* gene but suffered a severe truncation with the loss of ca. 50% of  
461 homologous bases compared to the functional *ndhC* gene of *M. coccinea* (KP205432, Kim et  
462 al., 2015).



463

464 **Figure 6:** Pattern of putative *ndh* gene degradation in *Dipodium*. Gene degradation plotted against the  
 465 maximum likelihood tree with focus on 24 fully assembled plastomes. (outgroups not shown). Support  
 466 values (SHaLRT/ UFboot) are shown on each branch. ps = pseudogenisation; *D. ham.* = *D.*  
 467 *hamiltonianum*

468

469 In *D. pandanum* 1, *D. stenocheilum* 1, and *D. variegatum* the *ndhF* gene was putatively lost  
 470 (**Figure 6**). All other samples possessed severely truncated *ndhF* genes with absent start codons  
 471 and multiple internal stop codons. The *ndhH* gene was present in *D. pandanum* 1 possessing a  
 472 length of 1,176 bp (99.2% of homologous length compared to *M. coccinea* (KP205432, Kim  
 473 et al., 2015). In most other samples, the *ndhH* gene was degraded possessing several stop  
 474 codons. *D. stenocheilum* 1 and *D. variegatum* lost the *ndhH* gene (**Figure 5**, **Figure 6**).

475 Moreover, *ndhE*, *ndhI* and *ndhA* were found to be putatively lost in the plastome of *D.*  
476 *variegatum* and *D. pandanum* 1, respectively (**Figure 5**, **Figure 6**). No gene loss occurred for  
477 *ndhB*, *ndhD* and *ndhJ*, however all three genes exhibited various degrees of degradation within  
478 all examined *Dipodium* plastomes and were either moderately or severely pseudogenised due  
479 to internal stop codons or frame-shift mutations.

480 The *ndhD* gene was found to have undergone the fewest degradation processes in regards of  
481 gene length which was largely conserved ranging from 1,122 bp (*D. campanulatum* 1) to 1,521  
482 bp (*D. pulchellum*) and in most plastomes *ndhD* possessed the alternative start codon ACG  
483 (Threonine). Furthermore, almost all *Dipodium* plastomes showed the canonical AUG  
484 (Methionine) start codon for *ndhA*, *ndhB*, *ndhE*, and *ndhI*. The intron-containing *ndhA* and  
485 *ndhB* genes exhibited the strongest degradation (i.e., large deletions) within the intron regions  
486 and the downstream exon in all *Dipodium* samples. Exon1 of *ndhB* was almost complete and  
487 in-frame for most plastomes and showed only one point mutation (from A to C) which resulted  
488 in a stop codon at amino acid position 68 (after 201 bp from the beginning of the first exon in  
489 *ndhB*).

490 Within different *Dipodium* complexes the patterns for putative *ndh* gene losses and severe or  
491 moderate pseudogenisations were similar for examined plastomes of *D. hamiltonianum* and *D.*  
492 *interaneum*. Both plastomes putatively lost *ndhG* and *ndhK* and showed severe  
493 pseudogenisations of *ndhA*, *ndhB*, *ndhC*, *ndhF*, *ndhH*, *ndhJ* and a moderately pseudogenised  
494 *ndhE* gene, but differed in level of putative pseudogenisation of *ndhD* and *ndhI* (**Figure 6**).

495 Other similarities were found in the *D. roseum* complex, in which the *ndhD* gene was  
496 moderately pseudogenised in all samples. Almost all samples of the *D. roseum* complex, except  
497 for *D. roseum* 2, harboured moderately pseudogenised *ndhE* and *ndhI* genes.

498 Within the same species, only *D. aff. roseum* 3 and *D. aff. roseum* 4 showed the same pattern  
499 of *ndh* gene loss and level of degradation which was also present in the plastome of *D.*  
500 *pardalinum* 2. Within the *D. stenocheilum* complex, *D. stenocheilum* 1 putatively lost *ndhI* and  
501 *ndhF*.

502 Across other samples, only two plastome pairs (*D. ensifolium* and *D. aff. roseum* 1; *D.*  
503 *basalticum*, and *D. atropurpureum* 2) shared the same pattern of *ndh* gene loss and degradation.  
504 In comparison to all other species of examined *Dipodium* plastomes, *D. variegatum*  
505 independently lost *ndhE* and *ndhI* and *D. pandanum* 1 lost the *ndhA* gene (**Figure 6**).

506  
507

## 508 4 Discussion

509 This is the first molecular study to elucidate interspecific relationships and divergence times in  
510 *Dipodium* and to examine plastid genome degradation within a mycoheterotrophic orchid  
511 genus of the Australasian flora in a phylogenomic context.

### 512 4.1 Phylogenetic placement and infrageneric relationships of *Dipodium*

513 This phylogenomic study based on 68 plastid loci provided strong support for the monophyly  
514 of *Dipodium* and its phylogenetic placement as an early diverging lineage within tribe  
515 Cymbidieae. Previous phylogenetic studies included only one or two species of *Dipodium*  
516 which precluded assessment of the monophyly of the genus (Pridgeon et al., 2009; Chase et  
517 al., 2015; Górnjak et al. (2010); Batista et al. (2014); Freudenstein and Chase (2015); Kim et  
518 al., 2020; Serna-Sánchez et al., 2021; McLay et al., 2023; Pérez-Escobar et al., 2023). Our  
519 study resolved *Dipodium* as the diverging early within Cymbidieae after subtribe Cymbidiinae  
520 with strong support and thus confirmed previous molecular phylogenetic studies in support of  
521 recognition of *Dipodium* at subtribal level as Dipodiinae (Li et al., 2016; Serna-Sánchez et al.,  
522 2021; Kim et al., 2020; Pérez-Escobar et al., 2023).

523 This phylogenomic study present the first molecular evidence in support of the infrageneric  
524 classification of *Dipodium* into sect. *Dipodium* and sect. *Leopardanthus* (O'Byrne, 2014;  
525 O'Byrne, 2017; Jones, 2021), lending support to the diagnostic value of vegetative traits (i.e.,  
526 the presence or absence of adventitious roots) in infrageneric classification of *Dipodium*.  
527 Section *Leopardanthus* is characterised by leafy species which possess adventitious roots, such  
528 as *Dipodium pandanum*. In contrast, sect. *Dipodium* comprises species without adventitious  
529 roots and includes all leafless species, the leafy species *D. ensifolium*, and the morphologically  
530 similar *D. gracile* from Sulawesi, the latter being only known from the type (destroyed)  
531 (O'Byrne, 2017). Our phylogenomic study supported the placement of the *D. ensifolium* in  
532 sect. *Dipodium*, resolved as sister to all leafless species in the section. However, further  
533 molecular study is warranted to ascertain the monophyly of the two sections based on an  
534 expanded sampling of sect. *Leopardanthus*.

535 Our phylogenomic study is the first to shed light on evolutionary relationships within sect.  
536 *Dipodium*, which was found to comprise six main lineages. The phylogenomic framework now  
537 allows assessment of useful diagnostic morphological traits to characterise main lineages  
538 within the section. For example, the yellow stem and flower colour of species of the *D.*  
539 *hamiltonianum* complex easily distinguishes this clade from other mycoheterotrophic orchids

540 within sect. *Dipodium* (**Figure 1**; Jones, 2021). Stems of remaining mycoheterotrophic species  
541 of sect. *Dipodium* are mostly greenish to dark reddish or purplish, whereas flowers vary in  
542 color from pale white, pinkish to purplish (**Figure 1**, Barrett et al., 2022; Jones, 2021). Also,  
543 sepal and petal characters were found to differ among clades: for example, species of clade A,  
544 comprising the *D. hamiltonianum* and *D. stenocheilum* complexes, possess sepals and lateral  
545 petals that are markedly narrower compared to species of clade B (comprising the *D. punctatum*  
546 and *D. roseum* complex) and *D. ensifolium*, the first diverging lineage within the sect.  
547 *Dipodium* (**Figure 1**; **Figure 3**) (Barrett et al., 2022; Jones, 2021).

548 Phylogenetic divergence within the two species complexes in clade B, *i.e.*, the *D. punctatum*  
549 and the *D. roseum* complexes, was shallow overall and thus interspecific relationships in these  
550 two groups remained largely unclear (**Figure 3**). Previous morphological studies highlighted  
551 difficulties in species delimitation within the *D. punctatum* complex, in particular between *D.*  
552 *pulchellum* and *D. punctatum* (Jones, 2021). While *D. pulchellum* is morphologically very  
553 similar to *D. punctatum*, the two species are differentiated by the intensity of their flower  
554 colours, which are richer in *D. pulchellum* and paler in *D. punctatum* (Jones and Clements,  
555 1987). However, a morphological study by Jones (2021) revealed that the strong floral  
556 coloration of *D. pulchellum* flowers was likely due to differences in environmental factors (*i.e.*,  
557 soil type and rainfall regime) of growing sites and thus Jones (2021) proposed to synonymise  
558 *D. pulchellum* with *D. punctatum*.

559 Similar challenges in taxonomic delimitation based on flower colours are also evident within  
560 the *D. roseum* complex. The distribution of the more widespread species *D. roseum* largely  
561 overlaps with the distributions of *D. atropurpureum* and *D. pardalinum* (ALA, 2023). Besides  
562 a very similar growing habit, the flowers of the three species are very similar in shape and vary  
563 only slightly in coloration: *D. roseum* has bright, rosy flowers with small darker spots, *D.*  
564 *atropurpureum* possesses dark pinkish-purple to dark reddish-purple flowers with spots and  
565 blotches, and the flowers of *D. pardalinum* are pale pink to white with large reddish spots and  
566 blotches (**Figure 1**) (Jones, 2021). Taken together, the overlapping distribution, similar  
567 appearance, and very shallow genetic divergence found in the present study among species in  
568 the *D. roseum* complex suggest that *D. atropurpureum* and *D. pardalinum* may be colour  
569 variations of *D. roseum*. Further molecular study with more highly resolving molecular  
570 techniques such as genotyping-by-sequencing is required to rigorously assess species  
571 delimitation within *Dipodium*.

572

## 573 4.2 Divergence-time estimations

574 Our divergence time estimations yielded results comparable to previous studies regarding the  
575 temporal diversification of major orchid clades (e.g., Givnish et al., 2015, Givnish et al., 2018;  
576 Kim et al., 2020; Serna-Sánchez et al., 2021; Zhang et al., 2023). Within Epidendroideae, this  
577 study confirmed that Cymbidieae was one of the most recently diverged tribes in Orchidaceae,  
578 consistent with previous studies (e.g., Givnish et al., 2015; Serna-Sánchez et al., 2021; Zhang  
579 et al., 2023). Stem and crown diversification of Cymbidieae were estimated to have  
580 commenced at ca. 42.2 Ma and 38.0 Ma respectively, which is similar to the estimates of Serna-  
581 Sánchez et al. (2021) and slightly younger than those of Zhang et al. (2023) (**Figure 4**,  
582 Supplementary Material 4 and 5).

583 Our study is the first to elucidate phylogenetic relationships and divergence times within  
584 *Dipodium*. Previously, only two studies included a representative of *Dipodium* (*D. roseum*,  
585 MN200368) in divergence-time estimations for Orchidaceae (Kim et al., 2020; Serna-Sánchez  
586 et al., 2021). These studies estimated the origin of *Dipodium* to ca. 17 Ma and ca. 31 Ma,  
587 respectively. Our study placed the divergence of *Dipodium* from the other subtribes in  
588 Cymbidieae to ca. 33.3 Ma in the early Oligocene which is closer to the findings of Serna-  
589 Sanchez et al. (2021). O’Byrne (2014) hypothesised that lineage divergence into sect.  
590 *Dipodium* and sect. *Leopardanthus* resulted from vicariance in conjunction with the break-up  
591 of Pangaea, in particular the separation of the Indian and Australian continental plates  
592 (O’Byrne, 2014). However, our divergence-time estimations show that *Dipodium* is far too  
593 young (< 33 Ma) to have been influenced by the break-up of Pangaea, which occurred from  
594 the early Jurassic and onwards. Lineage divergence of sect. *Dipodium* and sect. *Leopardanthus*  
595 were estimated to ca. 11.3 Ma in the late Miocene (**Figure 4**), when Australia had already  
596 assumed, approximately, its present geographical position. Rather, *Dipodium* is likely to have  
597 achieved its current distribution through range expansion between Australia and Southeast Asia  
598 across the Sunda-Sahul Convergence Zone (Joyce et al. 2021a), consistent with a general  
599 pattern of floristic exchange – the Sunda-Sahul Floristic Exchange - which was initiated as  
600 early as c. 30 Ma (Crayn et al., 2015; Joyce et al., 2021b). However, the data are insufficient  
601 at present to resolve the ancestral area of *Dipodium* and its main lineages. Further research is  
602 needed including an increased sampling to shed light on range evolution of *Dipodium* through  
603 ancestral range reconstruction.

604 Our results indicate that the Australian leafy species *D. ensifolium* diverged from the remainder  
605 of section *Dipodium* approximately 8.1 Ma (late Miocene) (**Figure 4**). The remainder of the

606 sect. *Dipodium* clade, which includes all leafless, putatively fully mycoheterotrophic species,  
607 emerged ca. 7.3 Ma (late Miocene) followed by rapid diversification from ca. 4.3 Ma onwards  
608 (early Pliocene) (**Figure 4**). Thus, mycoheterotrophy has most likely evolved only once within  
609 *Dipodium*, on the Australian continent during the late Miocene-early Pliocene.

610 From the late Miocene-early Pliocene (ca. 5 Ma) climatic conditions in Australia became  
611 increasingly arid, leading to a decline of rainforest vegetation and expansion of open  
612 sclerophyllous forests (Quilty, 1994, Gallagher et al., 2003, Martin, 2006, He and Wang, 2021).  
613 By the end of the Pliocene Australia's landscape was similar to the present day, with much of  
614 the continent a mosaic of open woody vegetation dominated by *Eucalyptus*, *Acacia* and  
615 Casuarinaceae (e.g., Martin 2006). The Pleistocene (ca. 2.58 – 0.012 Ma) was characterised by  
616 climatic oscillations which led to repeated forest expansion and contraction (Byrne, 2008). The  
617 evolution of mycoheterotrophy and the subsequent radiation of sect. *Dipodium* may have been  
618 facilitated by two factors: aridification in Australia favouring the reduction of leaf area to  
619 decrease water loss (O'Byrne, 2014), and the expansion of sclerophyll taxa and their  
620 mycorrhizal partners. Mycoheterotrophic *Dipodium* are assumed to share mycorrhizal fungi  
621 with Myrtaceae trees, especially *Eucalyptus*, (Bougoure and Dearnaley, 2005; Dearnaley and  
622 Le Brocque, 2006; Jones, 2021) which explosively diversified and came to dominate most  
623 Australian forests and presumably led to an increased diversity and abundance of suitable  
624 mycorrhizal partners for *Dipodium*. The rapid diversification of *Dipodium* from the Pleistocene  
625 onwards (ca. 3.2–0.3 Ma) (**Figure 4**) may have been driven by cycles of population  
626 fragmentation and coalescence in response to climatic oscillations.

## 627 **4.3 Plastid genome evolution**

### 628 **4.3.1 Plastome structural features and variations**

629 In this study, whole plastome assemblies were generated for 24 *Dipodium* samples, including  
630 representatives of all leafless, putatively full mycoheterotrophs of sect. *Dipodium* found in  
631 Australia, one leafy photosynthetic species of sect. *Dipodium* (*D. ensifolium*) and one leafy  
632 photosynthetic species of sect. *Leopardanthus* (*D. pandanum*). The overall organisation and  
633 the plastid gene content is generally conserved in most examined *Dipodium* plastomes (**Figure**  
634 **5, Table 2 and 3**). All examined plastomes showed the typical quadripartite structure of  
635 angiosperms (Ruhlman and Jansen 2014). However, some genomic features among several  
636 *Dipodium* plastomes were not conserved, including 1) differences in total genome length; 2)  
637 independent boundary shift IRB/SSC/IRA within the plastome of *D. pandanum* 1, *D.*  
638 *stenocheilum* 1, *D. variegatum*; 3) triplication of the *trnV*-GAC in the plastomes of *D.*



639 *ammolithum*, *D. elegantulum*, *D. hamiltonianum*, *D. stenocheilum* 2, *D. interaneum* 4) the  
640 independent pseudogenisation of *cemA* in the plastome of *D. aff. roseum* 4 and *trnD-GUC* in  
641 the plastome of *D. campanulatum* 1; and 5) the pseudogenisation or loss to varying degrees of  
642 *ndh* genes (**Figure 5**, **Table 3**, Supplementary Material 7).

643 Total genome length of *Dipodium* plastomes displayed differences of around 10,000 bp  
644 between the smallest (142,949 bp; *Dipodium variegatum*) and largest plastomes (152,956 bp  
645 *Dipodium aff. roseum* 3) which correlated with level of *ndh* gene degradation. Some *Dipodium*  
646 plastomes were similar to the average size of orchid plastomes (152,442 bp) published on NCBI  
647 database (286 Orchidaceae chloroplast genome, accessed on June 13, 2022), however most  
648 plastomes were smaller (average size *Dipodium* plastomes: 148,703 bp; **Table 2**). Average GC  
649 contents in *Dipodium* was very similar to the average GC content of published orchid plastomes  
650 on NCBI database (ca. 36.8%; 286 Orchidaceae chloroplast genome, accessed on June 13,  
651 2022) and all fell into the range of typical angiosperm plastomes (ca. 30–40%) (**Table 2**).

#### 652 **4.3.2 Patterns of *ndh* gene degradation within *Dipodium***

653 In orchids, *ndh* gene losses and pseudogenisations which occurred in both autotrophic and  
654 heterotrophic species have been documented in various genera (e.g., Kim et al., 2015; Feng et  
655 al., 2016; Niu et al., 2017; Barrett et al., 2018, Barrett et al., 2019; Roma et al., 2018; Lallemand  
656 et al., 2019; Kim et al., 2020; Peng et al., 2022; Kim et al., 2023). This study is in line with  
657 these general findings in that *ndh* gene degradation was also observed within the orchid genus  
658 *Dipodium*. All chloroplast *ndh* genes in *Dipodium* plastomes exhibited varying degrees of  
659 putative pseudogenisation and loss, not a single *ndh* gene remained functional among the  
660 examined chloroplast genomes (**Table 3**, **Figure 5**, **Figure 6**). These findings include all  
661 plastomes of leafless putatively fully mycoheterotrophic species and of two autotrophic leafy  
662 species (*D. pandanum* and *D. ensifolium*) and thus suggest that all examined species,  
663 independently of their nutritional status, have lost the functionality of the plastid NADH  
664 dehydrogenase complex. Hence, the last common ancestor of extant *Dipodium* is likely to have  
665 lacked a functional NDH complex. Previous studies in Cymbidiinae, the first diverging lineage  
666 in Cymbidieae, found that all species studied so far exhibited at least one degraded *ndh* gene  
667 (e.g., Yang et al., 2013; Kim and Chase 2017). As the next diverging lineage in Cymbidieae is  
668 *Dipodium*, this suggests that the degradation of *ndh* genes in Cymbidieae was likely a dynamic  
669 process from functional to non-functional. However, further research is needed e.g., ancestral  
670 state reconstructions of gene degradation with increased taxonomic sampling. The inclusion of

671 more species among sect. *Leopardanthus* is warranted to clarify if some *ndh* genes have  
672 remained functional in some autotrophic species of sect. *Leopardanthus*.

673 Previous studies examined *ndh* gene loss at genus level and revealed an independent loss of  
674 function of the NADH dehydrogenase complex for several genera (e.g., Lin et al., 2015, Kim  
675 et al., 2015). However, comparative whole plastome studies examining gene degradation and  
676 loss among closely related mycoheterotrophic species are still scarce. For a better  
677 understanding of *ndh* gene degradation patterns this study investigated the degree of *ndh* gene  
678 degradation among closely related orchid species (**Figure 6**). Greatest degradation within  
679 *Dipodium* were found for *ndhG* which is putatively lost in almost all examined plastomes,  
680 except *D. stenocheilum* 1 which retained a putative severely pseudogenised *ndhG* (**Figure 6**).  
681 The *ndhG* gene is located within the SSC region. In general, it is well established that genes in  
682 the SSC region experience higher substitution rates compared to genes located within IR  
683 regions (Ruhlman and Jansen 2014). The latter is the case for *ndhB* which is located in the IRs  
684 and structurally more conserved in *Dipodium* compared to most *ndh* genes located in the SSC.  
685 The greatest degree of *ndh* gene degradation occurred in *D. variegatum* which putatively lost  
686 *ndhC* and *ndhE–ndhI*. All other plastomes putatively lost at least one to three *ndh* genes and  
687 showed different levels of degradation (**Figure 6**).

688 Interestingly, the level of *ndh* gene degradation varied even among closely related species  
689 within species complexes. For example, *D. stenocheilum* 1 independently lost *ndhI* and *ndhF*,  
690 whereas all other studied samples of the *D. stenocheilum* complex retained those two genes as  
691 moderately or severely pseudogenised (**Figure 6**). Different levels of gene degradation and loss  
692 were even found within the same species. For example, *D. atropurpureum* 1 lost *ndhC* whereas  
693 *D. atropurpureum* 2 retained a severely pseudogenised *ndhC* (**Figure 6**). Moreover, the study  
694 of Kim et al., (2020) included one individual of *D. roseum* which showed a different pattern of  
695 *ndh* gene loss and degradation to those found among the *D. roseum* samples of this study. *D.*  
696 *roseum* (MN200386) experienced complete loss of *ndhA*, *ndhC–ndhI* and *ndhK*, but retained  
697 pseudogenised *ndhB* and *ndhJ* genes (Kim et al., 2020). These findings also agree with the  
698 recent comparative plastome study on *D. roseum* and *D. ensifolium*: *D. roseum* (OQ885084)  
699 has retained truncated *ndhB*, *ndhD* and *ndhJ* genes, but completely lost *ndhA*, *ndhC*, *ndhE–*  
700 *ndhI* and *ndhK* (McLay et al., 2023).

701 Overall, some patterns of *ndh* gene degradation found in this study in *Dipodium* are similar,  
702 however many were unique for each individual examined. Hence, this suggests that sect.  
703 *Dipodium* has undergone a recent and active *ndh* gene degradation which strongly implies a  
704 relaxed evolutionary selective pressure for the retention of the NDH complex.

### 705 4.3.3 IR/SSC junctions and IR instability

706 Orchidaceae plastomes frequently show an expansion/shift of the IR towards the SSC region  
707 (e.g., Kim et al., 2020). This instability of the IR/SSC junction is assumed to correlate with the  
708 deletion of *ndhF* and has resulted in a reduction of the SSC, as observed in several Orchidaceae  
709 plastomes (e.g., Kim et al., 2015; Niu et al., 2017; Dong et al., 2018; Roma et al., 2018) and in  
710 other land plant plastomes (e.g., Amaryllidaceae, Bignoniaceae, Orobanchaceae) (Thode and  
711 Lohmann 2019; Li et al., 2021; Könyves et al., 2021). This study revealed reduced SSC regions  
712 for most examined plastomes which correlated with the degradation of the *ndh* gene suite  
713 located in the SSC. Compared to typical SSC regions found in angiosperms (ca. 20 kb,  
714 Ruhlman and Jansen 2014), the smallest SSC region was reduced by ca. 7,900 bp (*D.*  
715 *variegatum*) and the largest SSC region was reduced by ca. 4,700 bp (*D. ensifolium*) (**Table 2**,  
716 **Figure 5**). However, a large expansion of the IR such as found in *Vanilla* and *Paphiopedilum*  
717 plastomes (Kim et al., 2015) was not found in *Dipodium* (IR sizes ranging between 24,436–  
718 26,817 bp, **Table 2**).

719 In angiosperms, the *ycf1* gene usually occupies ca. 1,000 bp in the IR (Sun et al., 2017, Kim et  
720 al., 2015). *Dipodium* plastomes in this study displayed varying positions of *ycf1* within the IR.  
721 In plastomes in which the *ndhF* gene was completely lost or severely truncated, the portion of  
722 *ycf1* within the IRA was mostly shorter compared to plastomes which contained moderately  
723 truncated *ndhF* genes (**Figure 5**). These results are similar with findings of Kim et al., (2015),  
724 a study which compared the locations of the IR/single-copy region junctions among 37 orchid  
725 plastomes and closely related taxa in Asparagales. In at least three plastomes (*D. pandanum* 1,  
726 *D. stenocheilum* 1, *D. variegatum*) *ndhF* was independently lost, the SSC/IRB junction was  
727 shifted into the spacer region near the *rpl32* gene in direct adjacency to the partially duplicated  
728 *ycf1* fragment (**Figure 5**, D, b–d). These findings suggest the deletion of *ndhF* correlated with  
729 the shift of the SSC/IRB junction. Interestingly, the boundaries between SSC and IR regions  
730 were found to be variable even among closely related species e.g., in *Cymbidium*. Some species  
731 in *Cymbidium* showed similar patterns of IR/SSC shifts (Kim and Chase 2017) as found in  
732 *Dipodium*.

733 In at least five plastomes (*D. ammolithum*, *D. elegantulum*, *D. hamiltonianum*, *D. interaneum*,  
734 *D. stenocheilum* 2) the *trnV*-GAC gene was triplicated (i.e., duplicated *trnV*-GAC version in  
735 close proximity to each other either in IRA or IRB) (**Figure 5**, B, C; **Table 3**). To the best of  
736 our knowledge, similar tRNA duplication patterns within the IR regions have not yet been  
737 found in any other Orchidaceae plastome. However, a recent study on plastomes of the  
738 angiosperm genus *Medicago* (Wu et al., 2021) yielded similar patterns. Wu et al. (2021) have

739 found three copies of the *trnV*-GAC gene in the plastomes of two closely related species within  
740 the IR (*M. archiducis-nicolai* and *M. ruthenica*) which were linked to forward and tandem  
741 repeats. Interestingly, Wu et al. (2021) findings support the hypothesis that repetitive sequences  
742 lead to genomic rearrangements and thus affect plastome stability. This may also apply for  
743 some *Dipodium* plastomes. However, to rule out any technical issues throughout the NGS  
744 process and to validate findings of duplicated tRNAs (and above-mentioned boundaries of  
745 IR/SC regions), PCR amplification of affected regions should be carried out in future studies.  
746 However, in strong support of tRNA duplication is their independent presence within the IR of  
747 five plastomes among individuals of the same species complexes (*D. stenocheilum* complex  
748 and *D. hamiltonianum* complex). However, an increased sampling is necessary to better  
749 understand the impacts of genomic rearrangements due to repetitive sequences and thus  
750 plastome instability in *Dipodium*.

#### 751 **4.3.4 Evolution of mycoheterotrophy and associated plastome degradation in** 752 ***Dipodium***

753 Heterotrophic plants are remarkable survivors, exhibiting often curious morphological,  
754 physical, or genomic modifications. Multiple heterotrophs were found to have suffered plastid  
755 genome degradations due to relaxed pressure on photosynthetic function. In recent years,  
756 evidence has accumulated that plastid genomes have undergone gene degradation in the  
757 evolutionary transition from autotrophy to heterotrophy (e.g., Graham et al., 2017; Barrett et  
758 al., 2019; Wicke et al., 2016). Among these, the first stage is the loss and pseudogenisation of  
759 genes involved in encoding the NDH complex. Interestingly, all examined plastomes of  
760 *Dipodium* have lost or pseudogenised all 11 *ndh* genes regardless of their nutritional status  
761 (**Figure 6**). Two photosynthetic species with green leaves were included in this study, *D.*  
762 *pandanum* (sect. *Leopardanthus*) and *D. ensifolium* (sect. *Dipodium*). Degradation in *ndh*  
763 genes among photosynthetic species is not surprising and was frequently reported in previous  
764 plastome studies in land plants. The large-scale study on Orchidaceae plastomes of Kim et al.,  
765 (2020) observed *ndh* gene pseudogenisation and losses among species in many epiphytes and  
766 several terrestrials which have retained their photosynthetic capacity. The NDH complex is  
767 thought to mediate the Photosystem I cyclic electron transport, fine-tunes photosynthetic  
768 processes and alleviates photooxidative stress (e.g., Yamori et al., 2015; Peltier et al., 2016;  
769 Sabater 2021). *D. pandanum* is a terrestrial or climbing epiphytic orchid and highly localised  
770 in rainforest habitats, whereas the terrestrial *D. ensifolium* grows in open forests and woodlands  
771 (Jones, 2021), thus both species seem to prefer shaded understory habitats. For epiphytic or  
772 terrestrial plants living in low-light habitats it has been proposed that the NDH complex may

773 not be essential anymore (e.g., Barrett et al., 2019). One reason for this may be that they are  
774 less exposed to photooxidative stress (e.g., Feng et al., 2016; Barrett et al., 2019). However,  
775 the NDH complex is composed of 11 chloroplast encoded subunits and additional subunits  
776 encoded by the nucleus (e.g., Peltier et al., 2016). It has been established that genomic material  
777 was repeatedly exchanged between the nucleus, mitochondrion, and chloroplast in the  
778 evolutionary course of endosymbiosis. Thus, previous studies examined whether genes were  
779 transferred from the chloroplast to the nucleus and/or mitochondrion genome or whether  
780 nuclear genes for the NDH complex suffered under degradation. Indeed, Lin et al., (2015)  
781 reported *ndh* fragments within the mitochondrial genomes of orchids, however no copies were  
782 found in the nuclear orchid genomes. Similar findings were reported from the orchid genus  
783 *Cymbidium* (Kim and Chase et al., 2017). However, further studies are needed to determine  
784 whether *ndh* gene transfer into the nucleus or mitochondrion may play a role within *Dipodium*.  
785 The proposed subsequent next steps toward (myco-) heterotrophy is the functional loss of  
786 photosynthetic genes (e.g., *psa*, *psb*, *pet*, *rbcL* or *rpo*) followed by genes for the chloroplast  
787 ATP synthase and genes with other function such as housekeeping genes (e.g., *matK*, *rpl*, *rnn*  
788 (e.g., Graham et al., 2017; Barrett et al., 2019). Most examined *Dipodium* plastomes displayed  
789 no additional plastid gene degradation besides *ndh* gene degradation, except in *D. aff. roseum*  
790 4 where *cemA* was pseudogenised and in *D. campanulatum* 1 where the *trnD-GUC* gene was  
791 pseudogenised (**Table 3**). The *cemA* gene encodes the chloroplast envelope membrane protein  
792 and was found to be non-essential for photosynthesis, however *cemA*-lacking mutants of the  
793 green alga *Chlamydomonas* were found to have a severely affected carbon uptake (Rolland et  
794 al., 1997) and may therefore be classified as directly involved in photosynthesis. Transfer RNA  
795 genes (*trn*) are involved in the translation process and categorised as ‘housekeeping’ genes  
796 (e.g., Graham et al., 2017; Wicke and Naumann 2018; Barrett et al., 2019). Moreover, similar  
797 gene degradation patterns were found in the plastomes of *D. roseum* (MN200386, Kim et al.,  
798 2020 and OQ885084, Mclay et al., 2023) and *D. ensifolium* (OQ885084, Mclay et al., 2023),  
799 which functionally lost all *ndh* genes. However, most photosynthesis related genes in the  
800 plastomes of *Dipodium* were found to be functional. Thus, mycoheterotrophic species of  
801 *Dipodium* display evidence of being at the beginning of plastid gene degradation, in contrast  
802 with the majority of fully mycoheterotrophic orchids which are in more advanced stages of  
803 degradation, e.g. *Cyrtosia septentrionalis* (Kim et al., 2019), *Epipogium* (Schelkunov et al.,  
804 2015), and *Rhizanthella* (Delannoy et al., 2011). On the other hand, mycoheterotrophs such as  
805 *Corallorhiza trifida* (Barrett et al., 2018), *Cymbidium macrorhizon* (Kim et al., 2017),  
806 *Hexalectris grandiflora* (Barrett et al., 2019) and *Limodorum abortivum* (Lallemand et al.,

807 2019) display functionally losses within the plastid *ndh* genes only and some species among  
808 them additionally lost one or two other genes, similar to findings in *Dipodium*. Interestingly,  
809 most of these species are leafless, but considered putatively partially mycoheterotrophic.  
810 Suetsugu et al. (2018) demonstrated that the leafless green orchid *Cymbidium macrorhizon*  
811 contains chlorophyll and can fix significant quantities of carbon during the fruit and seed  
812 production phase and thus, is photosynthetically active. Chlorophyll is present in *Corallorhiza*  
813 *trifida* also, but this green, leafless coralroot is an inefficient photosynthesiser (Barrett et al.,  
814 2014). Some species among leafless orchids within sect. *Dipodium* (e.g., *D. elegantulum*, *D.*  
815 *stenocheilum*, *D. variegatum*) appear green on stems (**Figure 1**, Jones 2021), which suggests  
816 they may contain some chlorophyll and be able to photosynthesise. Coupled with relatively  
817 mild plastid gene degradation compared to other fully mycoheterotrophic orchids, this suggests  
818 some leafless species among sect. *Dipodium* may be partially mycoheterotrophic rather than  
819 fully mycoheterotrophic as has been hypothesised for *D. roseum* (Kim et al. 2020; McLay et  
820 al. 2023). However, no studies so far have examined whether leafless species among sect.  
821 *Dipodium* contain chlorophyll and whether they are capable to carry out photosynthesis at  
822 sufficient rates. Therefore, more research is needed to assess the trophic status, including  
823 analysis of chlorophyll quantities and the ratio of photosynthetic carbon to fungal carbon for  
824 *Dipodium*.

825 Compared with recently published studies on mycoheterotrophic orchids such as *Corallorhiza*  
826 and *Hexalectris* (Barret et al. 2018; Barret et al. 2019) which incorporated divergence time  
827 estimations, plastomes of *Dipodium* showed the least degradation. *Hexalectris* crown age was  
828 estimated to ca. 24 Ma and plastomes of mycoheterotrophs were more degraded compared to  
829 mycoheterotrophic plastomes of *Corallorhiza* which diversified ca. 9 Ma onwards (Barret et  
830 al. 2018; Barret et al. 2019). *Dipodium* diversified in the late Miocene ca. 11 Ma, and the  
831 mycoheterotrophic lineage divergent from the autotrophic lineage ca. 8.1 Ma which is slightly  
832 younger compared to *Corallorhiza*. Hence, time of divergence may play a role in the degree of  
833 degradation of *Dipodium* plastomes which show an early stage of plastome degradation  
834 compared to older diverging mycoheterotrophic lineages that are in more advanced stages of  
835 plastome degradation.

## 836 **5 Conclusion**

837 This molecular phylogenomic comparative study clarified evolutionary relationships and  
838 divergence times of the genus *Dipodium* and provided support for two main lineages within

839 *Dipodium*, corresponding to the morphologically defined sect. *Dipodium* and sect.  
840 *Leopardanthus*. Phylogenetic analysis resolved the leafy autotroph *D. ensifolium* as being part  
841 of sect. *Dipodium* and found to be in sister group position to all leafless species in sect.  
842 *Dipodium*. Divergence-time estimations placed the divergence of the leafy species *D.*  
843 *ensifolium* from the remainder of section *Dipodium* in the late Miocene. Shortly after, the  
844 remaining clade including all leafless, putatively full mycoheterotrophic species within sect.  
845 *Dipodium* emerged ca. 7.3 Ma in the late Miocene followed by rapid species diversification  
846 from ca. 4.3 Ma onwards in the early Pliocene. Thus, this study indicates that  
847 mycoheterotrophy has most likely evolved only once on the Australian continent within  
848 *Dipodium* during the late Miocene, and that the ancestors of putatively full mycoheterotrophic  
849 species may have had green leaves. Among the examined plastomes, all plastid *ndh* genes were  
850 pseudogenised or physically lost, regardless of the individual's nutrition strategy (i.e.,  
851 autotroph versus mycoheterotroph). Thus, this study provides molecular evidence of relaxed  
852 evolutionary selective pressure on the retention of the NADH dehydrogenase complex.  
853 Mycoheterotrophic species among sect. *Dipodium* retained a full set of other functional  
854 photosynthesis-related genes and exhibited an early stage of plastid genome degradation.  
855 Hence, leafless species of sect. *Dipodium* may potentially be rather partially mycoheterotrophic  
856 than fully mycoheterotrophic.

857 To further disentangle evolutionary relationships in *Dipodium*, future studies based on nuclear  
858 data such as derived from target capture sequencing and with a denser sampling at population  
859 level are warranted. Moreover, the inclusion of a denser sampling of sect. *Leopardanthus* is  
860 warranted to clarify if some *ndh* genes may have remained functional in some of the autotrophic  
861 species of sect. *Leopardanthus*. To obtain further insights into the nutritional strategies in  
862 *Dipodium*, future studies should assess the trophic status of mycoheterotrophic species in  
863 *Dipodium* based on physiological data such as from the analysis of chlorophyll quantities and  
864 the ratio of photosynthetic carbon to fungal carbon for *Dipodium*. The Australian orchid flora  
865 harbours many more remarkable mycoheterotrophic lineages (e.g., *Danhatchia*) which offer  
866 the opportunity to further explore the evolutionary pathways to mycoheterotrophy and  
867 associated plastid genome evolution. The inclusion of autotrophic plants into comprehensive  
868 plastid phylogenetic analyses could broaden the understanding of the significance of observed  
869 *ndh* gene degradation patterns within Orchidaceae.

## Tables

**Table 1.** Plant material used in this study inclusive voucher details and provenances with botanical districts. Taxonomy according to the Australian Plant Census (APC, 2023). CANB = Australian National Herbarium, CNS = Australian Tropical Herbarium. AU = Australia, PG= Papua New Guinea. ACT = Australian Capital Territory, NT = Northern Territory, NSW = New South Wales, SA = South Australia, QLD = Queensland, WA = Western Australia, Vic = Victoria.

<b>Species</b>	<b>DNA extract No.</b>	<b>Voucher details</b>	<b>Provenance</b>
<i>Dipodium</i> aff. <i>roseum</i> 1	HTCG 0828	C. Bower ORG7817 (CANB 906470.1)	AU: NSW; Central Tablelands; Mullions Range State Forest
<i>Dipodium</i> aff. <i>roseum</i> 2	HTCG 0830	C. Bower ORG7818 WP 6 (CANB 906471.1)	AU: NSW; Central Tablelands; Mount Canobolas State Conservation Area
<i>Dipodium</i> aff. <i>roseum</i> 3	HTCG 0831	C. Bower ORG7818 WP 7 (CANB 906471.1)	AU: NSW; Central Tablelands; Mount Canobolas State Conservation Area
<i>Dipodium</i> aff. <i>roseum</i> 4	HTCG 0832	C. Bower ORG7818 WP 9,10,11 (CANB 906471.1)	AU: NSW; Central Tablelands; Mount Canobolas State Conservation Area
<i>Dipodium</i> aff. <i>stenocheilum</i>	HTCG 1691	D.L. Jones 8968 (CBG 9220253.1)	AU: QLD; Cook; Mount Elliot
<i>Dipodium</i> <i>ammolithum</i>	HTCG 1372	M.D. Barrett 4910A (PERTH)	AU: WA; North Kimberley, Theda Station
<i>Dipodium</i> <i>atropurpureum</i> 1	HTCG 0760	W.M. Dowling DC 1717 (CANB 924629.1)	AU: NSW; Northern Tablelands; Barrington Tops State Forest
<i>Dipodium</i> <i>atropurpureum</i> 2	HTCG 1679	M.A. Clements 4426 (CBG 8605570.1)	AU: NSW; Northern Tablelands; New England Highway to Armidale
<i>Dipodium</i> <i>basalticum</i>	HTCG 1693	D.E. Murfet 4837 (CANB 662327.1)	AU: NT; Darwin and Gulf; near Nhulunbuy
<i>Dipodium</i> <i>campanulatum</i> 1	HTCG 1680	K. Alcock DLJ5622 (CBG 9004646.2)	AU: SA; South-east; Naracoorte
<i>Dipodium</i> <i>campanulatum</i> 2	HTCG 1681	D.E. Murfet 1930b (CANB 677107.2)	AU: SA; South-east; Penola Conservation Park
<i>Dipodium</i> <i>elegantulum</i>	HTCG 1682	L. Lawler 8 (CBG 8605836.1)	AU: QLD; Cook; near Mareeba
<i>Dipodium</i> <i>ensifolium</i>	HTCG 1343	D.M. Crayn 1581 (CNS 145658.1)	AU: QLD; Cook; record is Queensland sensitive
<i>Dipodium</i> <i>hamiltonianum</i>	HTCG 1683	D.L. Jones & P.D. Jones s.n. (CANB)	AU: QLD; Moreton; Currimundi
<i>Dipodium</i> <i>interaneum</i>	HTCG 0181	J. Egan ORG7745 (CANB)	AU: ACT; Canberra; Birrigai
<i>Dipodium</i> <i>pandanum</i> 1	CNS_G01262	B. Gray 8233 (CANB 572368.2)	AU: QLD; Kennedy North; near Coen; record is Queensland sensitive



<i>Dipodium pandanum</i> 2	HTCG 1694	M. Jacobs 8984 (CANB 576763.1)	PG: Mount Bosavi
<i>Dipodium pardalinum</i> 1	HTCG 1684	D.L. Jones 12834 (CBG 9603749.1)	AU: Vic; Victorian Volcanic Plain; Heathmere
<i>Dipodium pardalinum</i> 2	HTCG 1685	D.L. Jones 12830 (CBG 9603745.1)	AU: Vic; Victorian Volcanic Plain; Heathmere
<i>Dipodium pulchellum</i>	HTCG 1686	D.L. Jones s.n. (CANB)	AU: QLD; Moreton; Green Mountains
<i>Dipodium punctatum</i>	HTCG 0827	C. Bower ORG7816 (CANB 906469.1)	AU: NSW; Central Tablelands; Black Salee Reserve
<i>Dipodium roseum</i> 1	HTCG 1687	C. Houston ORG3859 (CANB 656733.1)	AU: SA; Lofty South; Wotton Scrub
<i>Dipodium roseum</i> 2	HTCG 1688	C. Houston ORG3859 (CANB 656733.2)	AU: SA; Lofty South; Wotton Scrub
<i>Dipodium stenocheilum</i> 1	HTCG 1689	M.A. Clements 1189 (CBG 7801007.1)	AU: NT; Darwin and Gulf; Elcho Island
<i>Dipodium stenocheilum</i> 2	HTCG 1690	D.E. Murfet 3018 (CANB 619696.1)	AU: NT; Darwin and Gulf; Livingston
<i>Dipodium variegatum</i>	HTCG 1692	D.L. Jones 1280 (CANB 665182.1)	AU: QLD; Moreton; Beenleigh

### **Outgroup**

<i>Acriopsis emarginata</i>	CNS_G00305	C.D. Kilgour 634A (CNS 135324.1)	AU: QLD, Cook, Daintree National Park
<i>Cymbidium canaliculatum</i>	CNS_G00165	K.R. McDonald, 11722 (BRI AQ0831415)	AU: QLD, Cook, Mungkan Kandju National Park
<i>Eulophia bicallosa</i>	HTCG 1696	I. Morris (DLJ 4579) (CBG 8913381.1)	AU: NT; Darwin and Gulf; Howard Springs
<i>Eulophia graminea</i>	CNS_G02766	C.P. Brock 311 (CANB 596921.1)	AU: NT; Darwin
<i>Eulophia nuda</i>	HTCG 1697	R. Crane 1072 (CANB)	cult. ex AU: QLD; Moreton; Caloundra
<i>Geodorum densiflorum</i>	CNS_G01890	K. Schulte 254B (CNS 146066.1)	AU: QLD; Cairns region
<i>Oeceoclades pelorica</i>	HTCG 1695	J. Taylor s.n. (CBG 7905124.1)	cult. ex AU: QLD; Cook; Iron Range

**Table 2.** Comparison of plastome features in *Dipodium*.

Sample	Plastome Length (bp)	SSC length (bp)	IRA/B length (bp)	LSC length (bp)	GC content	Total CDS (unique CDS)	Total tRNA (unique tRNA)	Total rRNA (unique rRNA)	Total pseudo-genes	Total lost genes	Total functional genes
<i>D. pandanum</i> 1	146,204	13,849	24,762	82,831	37.0%	74 (68)	38 (30)	8 (4)	9	3	120
<i>D. ensifolium</i>	150,084	16,756	25,497	82,334	36.9%	74 (68)	38 (30)	8 (4)	10	3	120
<i>D. hamiltonianum</i> complex											
<i>D. hamiltonianum</i>	145,902	14,384	24,929	81,660	37.1%	74 (68)	39 (31)	8 (4)	10	3	121
<i>D. interaneum</i>	146,497	14,635	24,951	81,960	37.0%	74 (68)	39 (31)	8 (4)	10	3	121
<i>D. stenocheilum</i> complex											
<i>D. elegantulum</i>	144,865	14,003	24,606	81,650	36.9%	74 (68)	39 (31)	8 (4)	9	4	121
<i>D. stenocheilum</i> 2	145,589	13,821	25,127	81,514	37.0%	74 (68)	39 (31)	8 (4)	9	4	121
<i>D. stenocheilum</i> 1	144,751	12,670	25,009	82,063	36.9%	74 (68)	38 (30)	8 (4)	9	4	120
<i>D. basalticum</i>	148,478	15,238	25,640	81,960	37.0%	74 (68)	38 (30)	8 (4)	10	3	120
<i>D. ammolithum</i>	147,842	14,697	25,600	81,946	37.0%	74 (68)	39 (31)	8 (4)	9	4	121
<i>D. variegatum</i>	142,949	12,039	24,436	82,038	37.0%	74 (68)	38 (30)	8 (4)	6	7	120
<i>D. punctatum</i> complex											
<i>D. pulchellum</i>	151,425	15,735	26,369	82,952	36.9%	74 (68)	38 (30)	8 (4)	11	2	120
<i>D. punctatum</i>	151,181	15,737	26,136	83,172	37.0%	74 (68)	38 (30)	8 (4)	11	2	120
<i>D. campanulatum</i> 1	146,390	13,602	25,284	82,220	36.9%	74 (68)	37 (29)	8 (4)	12	2	119
<i>D. campanulatum</i> 2	149,050	14,266	25,902	82,980	37.0%	74 (68)	38 (30)	8 (4)	11	2	120
<i>D. roseum</i> complex											
<i>D. atropurpureum</i> 2	149,390	15,509	25,909	82,063	36.9%	74 (68)	38 (30)	8 (4)	10	3	120
<i>D. atropurpureum</i> 1	150,481	15,633	26,399	82,050	36.9%	74 (68)	38 (30)	8 (4)	9	4	120
<i>D. aff. roseum</i> 4	152,282	16,426	26,630	82,596	36.9%	73 (67)	38 (30)	8 (4)	11	3	119
<i>D. aff. roseum</i> 2	150,462	15,514	26,388	82,172	36.9%	74 (68)	38 (30)	8 (4)	9	4	120
<i>D. aff. roseum</i> 3	152,956	16,571	26,817	82,751	36.9%	74 (68)	38 (30)	8 (4)	10	3	120
<i>D. aff. roseum</i> 1	151,791	16,362	26,424	82,581	36.9%	74 (68)	38 (30)	8 (4)	10	3	120
<i>D. pardalinum</i> 2	151,659	16,276	26,580	82,223	36.9%	74 (68)	38 (30)	8 (4)	10	3	120
<i>D. pardalinum</i> 1	148,174	15,283	25,494	81,903	36.8%	74 (68)	38 (30)	8 (4)	9	4	120
<i>D. roseum</i> 1	150,857	15,848	26,521	81,967	36.9%	74 (68)	38 (30)	8 (4)	9	4	120
<i>D. roseum</i> 2	147,730	14,192	25,819	81,900	36.8%	74 (68)	38 (30)	8 (4)	9	4	120

1 **Table 3.** List of genes identified in the plastomes of *Dipodium*.

Gene group	Gene name
Transfer RNA genes	<i>trnA</i> -UGC <sup>*a</sup> , <i>trnC</i> -GCA, <i>trnD</i> -GUC <sup>d</sup> , <i>trnE</i> -UUC, <i>trnF</i> -GAA, <i>trnI</i> M-CAU, <i>trnG</i> -GCC, <i>trnG</i> -UCC <sup>*</sup> , <i>trnH</i> -GUG <sup>a</sup> , <i>trnI</i> -CAU <sup>a</sup> , <i>trnI</i> -GAU <sup>*a</sup> , <i>trnK</i> -UUU <sup>*</sup> , <i>trnL</i> -CAA <sup>a</sup> , <i>trnL</i> -UAA <sup>*</sup> , <i>trnL</i> -UAG, <i>trnM</i> -CAU, <i>trnN</i> -GUU <sup>a</sup> , <i>trnP</i> -UGG, <i>trnQ</i> -UUG, <i>trnR</i> -ACG <sup>a</sup> , <i>trnR</i> -UCU, <i>trnS</i> -GCU, <i>trnS</i> -GGA, <i>trnS</i> -UGA, <i>trnT</i> -GGU, <i>trnT</i> -UGU, <i>trnV</i> -GAC <sup>ab</sup> , <i>trnV</i> -UAC <sup>*</sup> , <i>trnW</i> -CCA, <i>trnY</i> -GUA
Small subunit of ribosome	<i>rps2</i> , <i>rps3</i> , <i>rps4</i> , <i>rps7</i> <sup>a</sup> , <i>rps8</i> , <i>rps11</i> , <i>rps12</i> <sup>*a</sup> , <i>rps14</i> , <i>rps15</i> , <i>rps16</i> <sup>*</sup> , <i>rps18</i> , <i>rps19</i> <sup>a</sup>
Large subunit of ribosome	<i>rpl2</i> <sup>*a</sup> , <i>rpl14</i> , <i>rpl16</i> <sup>*</sup> , <i>rpl20</i> , <i>rpl22</i> , <i>rpl23</i> <sup>a</sup> , <i>rpl32</i> , <i>rpl33</i> , <i>rpl36</i>
DNA-dependent RNA polymerase	<i>rpoA</i> , <i>rpoB</i> , <i>rpoC1</i> <sup>*</sup> , <i>rpoC2</i>
<b>Genes for photosynthesis</b>	
Subunits of photosynthesis I	<i>psaA</i> , <i>psaB</i> , <i>psaC</i> , <i>psaI</i> , <i>psaJ</i>
Subunits of photosynthesis II	<i>psbA</i> , <i>psbB</i> , <i>psbC</i> , <i>psbD</i> , <i>psbE</i> , <i>psbF</i> , <i>psbH</i> , <i>psbI</i> , <i>psbJ</i> , <i>psbK</i> , <i>psbL</i> , <i>psbM</i> , <i>psbN</i> , <i>psbT</i> , <i>psbZ</i>
Subunit of Cytochrome b6f	<i>petA</i> , <i>petB</i> <sup>*</sup> , <i>petD</i> <sup>*</sup> , <i>petG</i> , <i>petL</i> , <i>petN</i>
Subunit of ATP synthase	<i>atpA</i> , <i>atpB</i> , <i>atpE</i> , <i>atpF</i> <sup>*</sup> , <i>atpH</i> , <i>atpI</i>
Subunit of NADH dehydrogenase	<i>ndhA</i> <sup>*c</sup> , <i>ndhB</i> <sup>*ac</sup> , <i>ndhC</i> <sup>c</sup> , <i>ndhD</i> <sup>c</sup> , <i>ndhE</i> <sup>c</sup> , <i>ndhF</i> <sup>c</sup> , <i>ndhG</i> <sup>c</sup> , <i>ndhH</i> <sup>c</sup> , <i>ndhI</i> <sup>c</sup> , <i>ndhJ</i> <sup>c</sup> , <i>ndhK</i> <sup>c</sup>
Large subunits of RubisCO	<i>rbcL</i>
Ribosomal RNA genes	<i>rrn5</i> <sup>a</sup> , <i>rrn4.5</i> <sup>a</sup> , <i>rrn16</i> <sup>a</sup> , <i>rrn23</i> <sup>a</sup>
<b>Other genes</b>	
Maturase	<i>matK</i>
Envelope membrane protein	<i>cemA</i> <sup>c</sup>
Subunit of acetyl-CoA carboxylase	<i>accD</i>
C-type cytochrome synthesis gene	<i>cssA</i>
Protease	<i>clpP</i> <sup>*</sup>
Translation initiation factor IF-1	<i>infA</i>
<i>ycf</i> genes	<i>ycf1</i> , <i>ycf2</i> <sup>a</sup> , <i>ycf3</i> <sup>*</sup> , <i>ycf4</i>

2 <sup>a</sup>Duplicated gene. <sup>b</sup>Triplicated gene in *D. hamiltonianum*, *D. interaneum*, *D. elegantulum*, *D.*  
3 *stenocheilum* 2, *D. ammolithum*. <sup>c</sup>Pseudogene or lost. <sup>d</sup>Pseudogene in *D. campanulatum* 1. <sup>e</sup>Pseudogene  
4 in *D. aff. roseum* 4. \*Intron-containing gene.

5  
6  
7  
8  
9  
10  
11  
12  
13  
14

## 15 **Funding**

16 This study was supported by the Australian Biological Resources Study (Dept. of Agriculture,  
17 Water and the Environment, Australian Government NTRGP BBR210-34) and the Australian  
18 Orchid Foundation (AOF325.18; AOF357.23). SG received research grant from the Australian  
19 Tropical Herbarium.

## 20 **Conflict of Interest**

21 The authors declare that the research was conducted in the absence of any commercial or  
22 financial relationships that could be construed as a potential conflict of interest.

## 23 **Author Contributions**

24 **Conceptualisation:** SG, KN, MAC. **Methodology:** SG, KN, SJB; **Data curation:** SG, KN,  
25 MAC. **Formal analysis:** SG, SJB. **Funding acquisition:** KN, DMC, MAC, SG.  
26 **Investigation:** SG, KN, MAC, SJB, JAN, VSP, PMS. **Visualisation:** SG. **Writing – original**  
27 **draft:** SG. **Writing – review & editing:** SG, KN, MAC, SJB, JAN, VSP, PMS, DMC.

## 28 29 **Acknowledgements**

30 The authors acknowledge the contribution of Bioplatforms Australia (enabled by NCRIS) in  
31 the generation of data used in this publication. We acknowledge K. Alcock, M.D. Barrett, C.  
32 Bower, C.P. Brock, R. Crane, D.M. Crayn, W. Dowling, J. Egan, B. Gray, C. Houston, M.  
33 Jacobs, D.L. Jones, P.D. Jones, C.D. Kilgour, L. Lawler, K.R. McDonald, I. Morris, D.E.  
34 Murfet, J. Taylor for collection of plant material used in this study.

## 35 **Supplementary Material**

36 **Supplementary Material 1.** Details of samples included in phylogenetic analysis and  
37 divergence-time estimations.

38  
39 **Supplementary Material 2. a.** Details of plastid loci included in alignment of ML-  
40 phylogenetic and divergence-time estimations. **b.** Parsimony informative sites (Pi) for each  
41 plastid gene.

42  
43 **Supplementary Material 3.** ML-Phylogenetic tree of Orchidaceae.

44  
45 **Supplementary Material 4. a.** Model comparison by AICM (Akaike Information Criterion by  
46 MCMC) **b.** Comparison divergence-time estimations of major Orchidaceae lineages  
47 (subfamilies), the tribe Cymbidieae and subtribe Dipodiinae.

48

49 **Supplementary Material 5.** Maximum-clade-credibility tree from Bayesian divergence-time  
50 estimations of Orchidaceae.

51  
52 **Supplementary Material 6.** Summary of assembly features of 24 newly generated *Dipodium*  
53 plastomes.

54  
55 **Supplementary Material 7.** Circular plastome maps of 24 newly generated *Dipodium*  
56 plastomes.

57

## 58 **References**

59 ALA (2023). Atlas of Living Australia. Available at: <https://www.ala.org.au> (Accessed August,8  
60 2023).

61  
62 APC (2023): Australian Plant Census. Available at: [biodiversity.org.au/nsl/services/search/taxonomy](http://biodiversity.org.au/nsl/services/search/taxonomy)  
63 (Accessed May 5, 2023).

64  
65 Altschul, S.F., Gish, W., Miller, W., Myers, E.W., Lipman, D.J. (1990). Basic local alignment search  
66 tool. *J. Mol. Biol.* 215, 403–410. doi.org/10.1016/S0022-2836(05)80360-2

67  
68 Bankevich, A., Nurk, S., Antipov, D., Gurevich, A.A., Dvorkin, M., Kulikov, A.S., Lesin, V.M.,  
69 Nikolenko, S.I., Pham, S., Prjibelski, A.D., Pyshkin, A.V., Sirotkin, A.V., Vyahhi, N., Tesler, G.,  
70 Alekseyev, M.A., Pevzner, P.A. (2012). SPAdes: A new genome assembly algorithm and its  
71 applications to single-cell sequencing. *J. Comput. Biol.* 19, 455–477. doi.org/10.1089/cmb.2012.0021

72  
73 Barrett, C.F., Freudenstein, J.V., Li, J., Mayfield-Jones, D.R., Perez, L., Pires, J.C., Santos, C. (2014).  
74 Investigating the path of plastid genome degradation in an early-transitional clade of heterotrophic  
75 orchids, and implications for heterotrophic angiosperms. *Mol. Biol. Evol.* 31, 3095–3112.  
76 doi.org/10.1093/molbev/msu252

77  
78 Barrett, C.F., Wicke, S., Sass, C. (2018). Dense infraspecific sampling reveals rapid and independent  
79 trajectories of plastome degradation in a heterotrophic orchid complex. *New Phytol.* 218, 1192–1204.  
80 doi.org/10.1111/nph.15072

81  
82 Barrett, C.F., Sinn, B.T., Kennedy, A.H. (2019). Unprecedented parallel photosynthetic losses in a  
83 heterotrophic orchid genus. *Mol. Biol. Evol.* 36, 1884–1901. doi.org/10.1093/molbev/msz111

84  
85 Barrett, R. L., Barrett, M.D., Clements, M.A. (2022). A revision of Orchidaceae from the Kimberley  
86 region of Western Australia with new species of tropical *Calochilus* and *Dipodium*. *Telopea* 25, 203–  
87 270. doi.org/10.7751/telopea15711

88  
89 Batista, J.A.N., Mota, A.C.M., Proite, K., Bianchetti, L.D.B., Romero-González, G.A., Huerta, H.,  
90 Salazar, G.A. (2014). Molecular phylogenetics of neotropical *Cyanaeorchis* (Cymbidieae,  
91 Epidendroideae, Orchidaceae): geographical rather than morphological similarities plus a new species.  
92 *Phytotaxa* 156, 251–272. doi.org/10.11646/phytotaxa.156.5.1

93  
94 Bolger, A.M., Lohse, M., Usadel, B. (2014). Trimmomatic: a flexible trimmer for Illumina sequence  
95 data. *Bioinformatics* 30, 2114–2120. doi.org/10.1093/bioinformatics/btu170

96  
97 Bouckaert, R., Heled, J., Suchard, M.A., Rambaut, A., Drummond, A.J. (2014). BEAST 2: A software  
98 platform for Bayesian evolutionary analysis. *PLOS Comput. Biol.* 10, 4.  
99 doi.org/10.1371/journal.pcbi.1003537

- 100  
101 Bouckaert, R., Vaughan, T.G., Barido-Sottani, J., Duchêne, S., Fourment, M., Gavryushkina, A., Heled,  
102 J., Jones, G., Kühnert, D., De Maio, N., Matschiner, M., Mendes, F.K., Müller, N.F., Ogilvie, H.A., du  
103 Plessis, L., Poppinga, A., Rambaut, A., Rasmussen, D., Siveroni, I., Suchard, M.A., Wu, C.H., Xie, D.,  
104 Zhang, C., Stadler, T., Drummond, A.J. (2019). BEAST 2.5: An advanced software platform for  
105 Bayesian evolutionary analysis. *PLoS Comput. Biol.* 15, 4. doi.org/10.1371/journal.pcbi.1006650  
106  
107 Bougoure, J.J., Dearnaley, J.D.W (2005). The fungal endophytes of *Dipodium variegatum*  
108 (Orchidaceae). *Australasian Mycologist* 24, 15–19.  
109  
110 Bushnell, B. (2014). BBMap: A fast, accurate, splice-aware aligner. Lawrence Berkeley National  
111 Laboratory, Berkeley, CA (United States).  
112  
113 Braukmann, T.W.A., Broe, M.B., Stefanović, S. and Freudenstein, J.V. (2017). On the brink: the highly  
114 reduced plastomes of nonphotosynthetic Ericaceae. *New Phytol.* 216, 254-266.  
115 doi.org/10.1111/nph.14681  
116  
117 Byrne, M., Yeates, D.K., Joseph, L., Kearney, M., Bowler, J., Williams, M.A.J., Cooper, S., Donnellan,  
118 S.C., Keogh, J.S., Leys, R., Melville, J., Murphy, D.J., Porch, N. and Wyrwoll, K.-H. (2008). Birth of  
119 a biome: insights into the assembly and maintenance of the Australian arid zone biota. *Mol. Ecol.* 17,  
120 4398–4417. doi.org/10.1111/j.1365-294X.2008.03899.x  
121  
122 Chase, M.W., Cameron, K.M., Freudenstein, J.V., Pridgeon, A.M., Salazar, G., Van den Berg C.,  
123 Schuiteman, A. (2015). An updated classification of Orchidaceae. *Bot. J. Linn. Soc.* 177, 151–174.  
124 doi.org/10.1111/boj.12234  
125  
126 Christenhusz, M.J.M, Byng, J.W. (2016). The number of known plants species in the world and its  
127 annual increase. *Phytotaxa* 261, 201. doi.org/10.11646/phytotaxa.261.3.1.  
128  
129 Crayn, D.M., Costion, C., Harrington, M.G. (2015). The Sahul–Sunda floristic exchange: dated  
130 molecular phylogenies document Cenozoic intercontinental dispersal dynamics. *J. Biogeog.* 42, 11–24.  
131 dx.doi.org/10.1111/jbi.12405  
132  
133 Dearnaley, J.D.W., Le Brocq, A.F. (2006). Molecular identification of the primary root fungal  
134 endophytes of *Dipodium hamiltonianum* (Orchidaceae). *Aust. J. Bot.* 54, 487.  
135 doi.org/10.1071/BT05149  
136  
137 Delannoy, E., Fujii, S., Colas des Francs-Small, C., Brundrett, M., Small, I. (2011). Rampant gene loss  
138 in the underground orchid *Rhizanthella gardneri* highlights evolutionary constraints on plastid  
139 genomes. *Mol. Biol. Evol.* 28, 2077–2086. doi.org/10.1093/molbev/msr028  
140  
141 Douglas, J., Zhang, R., Bouckaert, R. (2021). Adaptive dating and fast proposals: Revisiting the  
142 phylogenetic relaxed clock model. *PLoS Comput. Biol.* 17 (2). doi.org/10.1371/journal.pcbi.1008322  
143  
144 Dong, W.L., Wang, R.N., Zhang, N.Y., Fan, W.B., Fang, M.F., Li, Z.H. (2018). Molecular evolution  
145 of chloroplast genomes of orchid species: insights into phylogenetic relationship and adaptive  
146 evolution. *Int. J. Mol. Sci.* 19, 716. doi.org/10.3390/ijms19030716  
147  
148 Drummond, A.J., Rambaut, A. (2007). BEAST: Bayesian evolutionary analysis by sampling trees.  
149 *BMC Evol. Biol.* 7, 214. doi.org/10.1186/1471-2148-7-214  
150  
151 Fabozzi, F.J., Focardi, S.M., Rachev, S.T., Arshanapalli, B.G. (2014). Appendix E. Model Selection  
152 Criterion: AIC and BIC in “The basics of financial econometrics: tools, concepts, and asset management  
153 applications.” John Wiley & Sons, Inc. 399–403.  
154

- 155 Feng, Y.L., Wicke, S., Li, J.W., Han, Y., Lin, C.S., Li, D.Z., Zhou, T.T., Huang, W.C., Huang, L.Q.,  
156 Jin, X.H. (2016). Lineage-specific reductions of plastid genomes in an orchid tribe with partially and  
157 fully mycoheterotrophic species. *Genome Biol. Evol.* 8, 2164–2175. doi.org/10.1093/gbe/evw144  
158
- 159 Freudenstein, J.V., Chase, M.W. (2015). Phylogenetic relationships in Epidendroideae (Orchidaceae),  
160 one of the great flowering plant radiations: progressive specialization and diversification. *Ann. Bot.* 115,  
161 665–681. doi.org/10.1093/aob/mcu253  
162
- 163 Gallagher, S.J., Greenwood, D.R., Taylor, D., Smith, A.J., Wallace, M.W., Holdgate, G.R. (2003). The  
164 Pliocene climatic and environmental evolution of southeastern Australia: Evidence from the marine and  
165 terrestrial realm. *Palaeogeogr., Palaeoclimatol., Palaeoecol.* 193, 349–382.  
166 doi.org/10.1016/S0031-0182(03)00231-1  
167
- 168 Gernhard, T. (2008). The conditioned reconstructed process. *J. Theor. Biol.* 253, 769–778.  
169 doi.org/10.1016/j.jtbi.2008.04.005  
170
- 171 Givnish, T.J., Zuluaga, A., Spalink, D., Soto Gomez, M., Lam, V.K.Y., Saarela, J.M., Sass, C., Iles,  
172 W.J.D., De Sousa, D.J.L., Leebens-Mack, J., Chris Pires, J., Zomlefer, W.B., Gandolfo, M.A., Davis,  
173 J.I., Stevenson, D.W., De Pamphilis, C., Specht, C.D., Graham, S.W., Barrett, C.F., Ané, C. (2018).  
174 Monocot plastid phylogenomics, timeline, net rates of species diversification, the power of multi-gene  
175 analyses, and a functional model for the origin of monocots. *Am. J. Bot.* 105, 1888–1910.  
176 doi.org/10.1002/ajb2.1178  
177
- 178 Givnish, T.J., Spalink, D., Ames, M., Lyon, S.P., Hunter, S.J., Zuluaga, A., Iles, W.J.D., Clements,  
179 M.A., Arroyo, M.T.K., Leebens-Mack, J., Endara, L., Kriebel, R., Neubig, K.M., Whitten, W.M.,  
180 Williams, N.H., Cameron, K.M. (2015). Orchid phylogenomics and multiple drivers of their  
181 extraordinary diversification. *Proc. Royal Soc. B* 282, 20151553. doi.org/10.1098/rspb.2015.1553  
182
- 183 Górniak, M., Paun, O., Chase, M.W. (2010). Phylogenetic relationships within Orchidaceae based on a  
184 low-copy nuclear coding gene, *Xdh*: Congruence with organellar and nuclear ribosomal DNA results.  
185 *Mol. Phy. Evol.* 56, 784–795. doi.org/10.1016/j.ympev.2010.03.003  
186
- 187 Graham, S.W., Lam, V.K.Y., Merckx, V.S.F.T (2017). Plastomes on the edge: the evolutionary  
188 breakdown of mycoheterotroph plastid genomes. *New Phytol.* 214, 48–55. doi.org/10.1111/nph.14398  
189
- 190 Greiner, S., Lehwark, P., Bock, R. (2019). OrganellarGenomeDRAW (OGDRAW) version 1.3.1:  
191 expanded toolkit for the graphical visualization of organellar genomes. *Nucleic Acids Res.* 47, W59–  
192 W64. doi.org/10.1093/nar/gkz238  
193
- 194 Guindon, S., Dufayard, J.-F., Lefort, V., Anisimova, M., Hordijk, W., Gascuel, O. (2010). New  
195 algorithms and methods to estimate maximum-likelihood phylogenies: Assessing the performance of  
196 PhyML 3.0. *Syst. Biol.* 59, 307–321. doi.org/10.1093/sysbio/syq010  
197
- 198 He, Y., Wang, H. (2021). Terrestrial material input to the northwest shelf of Australia through the  
199 Pliocene-Pleistocene period and its implications on continental climates. *Geophys. Res. Lett.*, 48,  
200 e2021GL092745. doi.org/10.1029/2021GL092745  
201
- 202 Hoang, D.T., Chernomor, O., Von Haeseler, A., Minh, B.Q., Vinh, L.S. (2018). UFBoot2: Improving  
203 the Ultrafast Bootstrap approximation. *Mol. Biol. Evol.* 35, 518–522. doi.org/10.1093/molbev/msx281  
204
- 205 Jacquemyn, H., Merckx, V.S.F.T (2019). Mycorrhizal symbioses and the evolution of trophic modes in  
206 plants (R Shefferson, Ed.). *J. Ecol.* 107, 1567–1581. doi.org/10.1111/1365-2745.13165  
207
- 208 Jones, D.L. (2021). A complete guide to native orchids of Australia. Sydney: Reed New Holland  
209 Publishers.

- 210  
211 Jones, D.L. and Clements, M.A. (1987). New orchid taxa from south-eastern Queensland. *Proc. R. Soc.*  
212 *Queensland* 98, 128.  
213  
214 Joyce, E.M., Crayn, D.M., Lam, V.K.Y., Gerelle, W.K., Graham, S.W., Nauheimer, L. (2018). Evolution  
215 of *Geosiris* (Iridaceae): historical biogeography and plastid-genome evolution in a genus of non-  
216 photosynthetic tropical rainforest herbs disjunct across the Indian Ocean. *Aust. Syst. Bot.* 31, 504–522.  
217 doi.org/10.1071/SB18028  
218  
219 Joyce, E.M., Thiele, K.R., Slik, J.W.F., Crayn, D.M. (2021a). Plants will cross the lines: climate and  
220 available land mass are the major determinants of phytogeographical patterns in the Sunda–Sahul  
221 Convergence Zone. *Biol. J. Linn. Soc.* 132, 374–387. doi.org/10.1093/biolinnean/blaa194  
222  
223 Joyce, E.M., Pannell, C.M., Rossetto, M., Yap, J.Y.S., Thiele, K.R., Wilson, P.D., Crayn, D.M. (2021b).  
224 Molecular phylogeography reveals two geographically and temporally separated floristic exchange  
225 tracks between Southeast Asia and Northern Australia. *J. Biogeog.* 48, 1213–1227.  
226 doi.org/10.1111/jbi.14072  
227  
228 Kalyanamoorthy, S., Minh, B.Q., Wong, T.K.F., Von Haeseler, A., Jermini, L.S. (2017). ModelFinder:  
229 fast model selection for accurate phylogenetic estimates. *Nat. Methods* 14, 587–589.  
230 doi.org/10.1038/nmeth.4285  
231  
232 Katoh, K., Misawa, K., Kuma, K., Miyata, T., MAFFT (2002). A novel method for rapid multiple  
233 sequence alignment based on fast Fourier transform, *Nucleic Acids Res.* 30 (14), 3059–3066,  
234 doi.org/10.1093/nar/gkf436  
235  
236 Katoh, K., Standley, D.M. (2013). MAFFT Multiple Sequence Alignment Software Version 7:  
237 Improvements in performance and usability. *Mol. Biol. Evol.* 30, 772–780.  
238 <https://doi.org/10.1093/molbev/mst010>  
239  
240 Kim, H.T., Kim, J.S., Moore, M.J., Neubig, K.M., Williams, N.H., Whitten, W.M., Kim, J.H. (2015).  
241 Seven new complete plastome sequences reveal rampant independent loss of the *ndh* gene family across  
242 orchids and associated instability of the inverted repeat/small single-copy region Boundaries (S. Aceto,  
243 Ed.). *PLOS ONE* 10, e0142215. doi.org/10.1371/journal.pone.0142215  
244  
245 Kim, H.T., Chase, M.W. (2017). Independent degradation in genes of the plastid *ndh* gene family in  
246 species of the orchid genus *Cymbidium* (Orchidaceae; Epidendroideae). *PLOS ONE* 12, e0187318.  
247 doi.org/10.1371/journal.pone.0187318  
248  
249 Kim, Y.K., Kwak, M.H., Chung, M.G., Kim, H.W., Jo, S., Sohn, J.Y., Cheon, S.H., Kim, K.J. (2017)  
250 The complete plastome sequence of the endangered orchid *Cymbidium macrorhizon* (Orchidaceae).  
251 *Mitochondrial DNA Part B* 2, 725–727. doi.org/10.1080/23802359.2017.1390411  
252  
253 Kim, Y.K., Jo, S., Cheon, S.H., Joo, M.J., Hong, J.R., Kwak, M.H., Kim, K.J. (2019). Extensive losses  
254 of photosynthesis genes in the plastome of a mycoheterotrophic orchid, *Cyrtosia septentrionalis*  
255 (Vanilloideae: Orchidaceae). *Genome Biol. Evol.* 11(2), 565–571. <https://doi.org/10.1093/gbe/evz024>  
256  
257 Kim, Y.K., Jo, S., Cheon, S.H., Joo, M.J., Hong, J.R., Kwak, M., Kim, K.J. (2020). Plastome evolution  
258 and phylogeny of Orchidaceae, with 24 new sequences. *Front. Plant Sci.* 11, 22.  
259 <https://doi.org/10.3389/fpls.2020.00022>  
260  
261 Kim, Y.K., Cheon, S.-H., Hong, J.-R., Kim, K.J. (2023). Evolutionary Patterns of the Chloroplast  
262 Genome in Vanilloid Orchids (Vanilloideae, Orchidaceae). *Int. J. Mol. Sci.* 24, 3808.  
263 doi.org/10.3390/ijms24043808  
264



- 265 Klimpert, N.J., Mayer, J.L.S., Sarzi, D.S., Prosdocimi, F., Pinheiro, F., Graham, S.W. (2022).  
266 Phylogenomics and plastome evolution of a Brazilian mycoheterotrophic orchid, *Pogoniopsis*  
267 *schenckii*. *Am. J. Bot.* 109(12), 2030–2050. doi.org/10.1002/ajb2.16084  
268
- 269 Könyves, K., Bilsborrow, J., Christodoulou, M.D., Culham, A., David, J. (2021). Comparative  
270 plastomics of Amaryllidaceae: inverted repeat expansion and the degradation of the *ndh* genes in  
271 *Strumaria truncate* Jacq. *PeerJ* 9, e12400. doi.org/10.7717/peerj.12400  
272
- 273 Lam, V.K.Y., Gomez, M.S., Graham, S.W. (2015). The highly reduced plastome of mycoheterotrophic  
274 *Sciaphila* (Triuridaceae) is colinear with its green relatives and is under strong purifying selection,  
275 *Genome Biol. Evol.* 7, 2220–2236. <https://doi.org/10.1093/gbe/evv134>  
276
- 277 Lallemand, F., Logacheva, M., Le Clainche, I., Bérard, A., Zheleznaia, E., May, M., Jakalski, M.,  
278 Delannoy, É., Le Paslier, M.C., Selosse, M.A. (2019). Thirteen new plastid genomes from mixotrophic  
279 and autotrophic species provide insights into heterotrophy evolution in Neottieae orchids. *Genome Biol.*  
280 *Evol.* 11, 2457–2467. doi.org/10.1093/gbe/evz170  
281
- 282 Li, M.H., Zhang, G.Q., Liu, Z.J., Lan, S.R. (2016). Subtribal relationships in Cymbidieae  
283 (Epidendroideae, Orchidaceae) reveal a new subtribe, Dipodiinae, based on plastid and nuclear coding  
284 DNA. *Phytotaxa* 246, 37. doi.org/10.11646/phytotaxa.246.1.3  
285
- 286 Li, X., Yang, J.B., Wang, H., Song, Y., Corlett, R.T., Yao, X., Li, D.Z., Yu, W.B. (2021). Plastid NDH  
287 pseudogenization and gene loss in a recently derived lineage from the largest hemiparasitic plant genus  
288 *Pedicularis* (Orobanchaceae). *Plant Cell Physiol.* 62, 971–984. doi.org/10.1093/pcp/pcab074  
289
- 290 Li, Z.H., Jiang, Y., Ma, X., Li, J.W., Yang, J.B., Wu, J.Y., Jin, X.H. (2020). Plastid genome evolution  
291 in the subtribe Calypsoinae (Epidendroideae, Orchidaceae) (J Archibald, Ed.). *Genome Biol. Evol.* 12,  
292 867–870. doi.org/10.1093/gbe/evaa091  
293
- 294 Lin, C.S., Chen, J.J., Huang, Y.T., Chan, M.T., Daniell, H., Chang, W.J., Hsu, C.T., Liao, D.C., Wu,  
295 F.H., Lin, S.Y., Liao, C.F., Deyholos, M.K., Wong, G.K., Albert, V.A., Chou, M.L., Chen, C.Y., Shih,  
296 M.C. (2015). The location and translocation of *ndh* genes of chloroplast origin in the Orchidaceae  
297 family. *Sci. Rep.* 12; 5:9040. doi.org/10.1038/srep09040  
298
- 299 Logacheva, M.D., Schelkunov, M.I., Aleksey, A. P. (2011). Sequencing and analysis of plastid genome  
300 in mycoheterotrophic orchid *Neottia nidus-avis*. *Genome Biol. Evol.* 3, 1296–1303.  
301 doi.org/10.1093/gbe/evr102  
302
- 303 Martin, H.A. (2006). Cenozoic climatic change and the development of the arid vegetation in Australia.  
304 *J. Arid Environ.* 66, 533–563. doi.org/10.1016/j.jaridenv.2006.01.009  
305
- 306 McLay, T.G. B., Bayly, M. J., Whitehead, M. R., Fowler, R. M. (2023). Retention of an apparently  
307 functional plastome in an apparently mycoheterotrophic orchid, *Dipodium roseum* D.L.Jones &  
308 M.A.Clem. (Orchidaceae). *Aust. J. Bot.* 71, 306–317. doi.org/10.1071/BT22075  
309
- 310 Merckx, V.S.F.T. (2013). *Mycoheterotrophy: an introduction in Mycoheterotrophy. The Biology of*  
311 *Plants Living on Fungi*. Berlin: Springer-Verlag 297–342.  
312 doi.org/10.1007/978-1-4614-5209-6  
313
- 314 Minh, B.Q., Schmidt, H.A., Chernomor, O., Schrempf, D., Woodhams, M.D., Von Haeseler, A.,  
315 Lanfear, R. (2020). IQ-TREE 2: New Models and efficient methods for phylogenetic inference in the  
316 genomic era. *Mol. Biol. Evol.* 37, 1530–1534. doi.org/10.1093/molbev/msaa015  
317

- 318 Nargar, K., O'Hara, K., Mertin, A., Bent, S.J., Nauheimer, L., Simpson, L., Zimmer, H., Molloy, B.P.J.,  
319 Clements, M.A. (2022). Evolutionary relationships and range evolution of greenhood orchids (subtribe  
320 Pterostylidinae): Insights from plastid phylogenomics. *Front. Plant Sci.* 13:912089.  
321 [doi.org/10.3389/fpls.2022.912089](https://doi.org/10.3389/fpls.2022.912089)  
322
- 323 NCBI (2022), National Library of Medicine. Available at: <https://www.ncbi.nlm.nih.gov> (Accessed  
324 June 2, 2022)  
325
- 326 Nguyen, L.T., Schmidt, H.A., Von Haeseler, A., Minh, B.Q. (2015). IQ-TREE: A fast and effective  
327 stochastic algorithm for estimating maximum-likelihood phylogenies. *Mol. Biol. Evol.* 32, 268–274.  
328 [doi.org/10.1093/molbev/msu300](https://doi.org/10.1093/molbev/msu300)  
329
- 330 Niu, Z., Xue, Q., Zhu, S., Sun, J., Liu, W., Ding, X. (2017). The complete plastome sequences of four  
331 orchid species: Insights into the evolution of the Orchidaceae and the utility of plastomic mutational  
332 hotspots. *Front. Plant Sci.* 8, 715. [doi.org/10.3389/fpls.2017.00715](https://doi.org/10.3389/fpls.2017.00715)  
333
- 334 O'Byrne, P. (2014). On the evolution of *Dipodium* R. Br. *Reinwardtia* 14 (1), 123–132 [https://e-](https://e-journal.biologi.lipi.go.id/index.php/reinwardtia/article/view/402)  
335 [journal.biologi.lipi.go.id/index.php/reinwardtia/article/view/402](https://e-journal.biologi.lipi.go.id/index.php/reinwardtia/article/view/402) (Accessed November 22, 2021)  
336
- 337 O'Byrne, P. (2017). A taxonomic revision of *Dipodium* section *Leopardanthus*. *Malesian Orchid*  
338 *Journal* 19, 5–142.  
339
- 340 Peltier, G., Aro, E-M., Shikanai, T. (2016). NDH-1 and NDH-2 plastoquinone reductases in oxygenic  
341 photosynthesis. *Ann. Rev. Plant Biology* 67, 55–80. [doi.org/10.1146/annurev-arplant-043014-114752](https://doi.org/10.1146/annurev-arplant-043014-114752)  
342
- 343 Peng, H.-W., Lian, L. Zhang, J., Erst A.S., Wang, W. (2022). Phylogenomics, plastome degradation  
344 and mycoheterotrophy evolution of Neottieae (Orchidaceae), with emphasis on the systematic position  
345 and Loess Plateau-Changbai Mountains disjunction of *Diplandrorchis*. *BMC Plant Biol.* 22, 5077.  
346 [doi.org/10.1186/s12870-022-03906-0](https://doi.org/10.1186/s12870-022-03906-0)  
347
- 348 Pérez-Escobar, O. A, Bogarín, D., Przelomska, N.A.S., Ackerman, J.D., Balbuena, J.A., Bellot, S.  
349 Bühlmann, R. P., Cabrera, B., Aguilar Cano, J. , Charitonidou, M., Chomicki, G., Clements, M.A.,  
350 Cribb, P., Fernández, M., Flanagan, N.S., Gravendeel, B., Hágsater, E., Halley, J.M., Hu, A.-Q.,  
351 Jaramillo, C., Mauad, A.V., Maurin, O., Müntz, R., Leitch, I.J., Li, L., Negrao, R., Oses, L., Phillips,  
352 C., Rincon, M. Salazar-Chavez, G., Simpson, L., Smidt, E., Solano-Gomez, R., Parra-Sánchez, E.,  
353 Tremblay, R.L., van den Berg, C., Villanueva, B.S., Zuluaga, A., Chase, M.W., Fay, M.F., Condamine,  
354 M.F., Forest, F. Nargar, N., Renner, S. S., Baker, W.J., Antonelli, A. (2023). The origin and speciation  
355 of orchids [Preprint]. Available at <https://www.biorxiv.org/content/10.1101/2023.09.10.556973v3.full>,  
356 (Accessed January 3, 2024). [doi.org/10.1101/2023.09.10.556973](https://doi.org/10.1101/2023.09.10.556973)  
357
- 358 POWO (2023). Plants of the World Online. Facilitated by the Royal Botanic Gardens, Kew. Published  
359 on the Internet; <http://www.plantsoftheworldonline.org/> (Accessed September 8, 2023).  
360
- 361 Pridgeon, A.M., Cribb, P.J., Chase, M.W., Rasmussen, F.N. et al. (2009). Genera Orchidacearum,  
362 Volume 5, Epidendroideae (Part 2). Oxford University, Oxford (New York), 585.  
363
- 364 Qu, X.J., Fan, S.J., Wicke, S., Yi, T.S. (2019). Plastome reduction in the only parasitic gymnosperm  
365 *Parasitaxus* is due to losses of photosynthesis but not housekeeping genes and apparently involves the  
366 secondary gain of a Large Inverted Repeat. *Genome Biol. Evol.* 11(10). 2789–2796.  
367 [doi.org/10.1093/gbe/evz187](https://doi.org/10.1093/gbe/evz187)  
368
- 369 Quilty, P.G. (1994). The background: 144 million years of Australian paleoclimate and  
370 palaeogeography. In 'History of the Australian vegetation: Cretaceous to recent'. 14–39. 2017 Edition.  
371 (Cambridge University Press: Cambridge, UK). [doi.org/10.20851/australian-vegetation](https://doi.org/10.20851/australian-vegetation)  
372

- 373 Rambaut, A., Drummond, A.J., Xie, D., Baele, G., Suchard, M.A. (2018). Posterior summarization in  
374 Bayesian phylogenetics using Tracer 1.7. *Syst. Biol.* 67, 901–904. doi.org/10.1093/sysbio/syy032  
375
- 376 Rolland, N., Dorne, A.J., Amoroso, G., Sültemeyer, D.F., Joyard, J., Rochaix, J.D. (1997). Disruption  
377 of the plastid *ycf10* open reading frame affects uptake of inorganic carbon in the chloroplast of  
378 *Chlamydomonas*. *EMBO J.* 16, 6713–6726. doi.org/10.1093/emboj/16.22.6713  
379
- 380 Roma, L., Cozzolino, S., Schlüter, P.M., Scopece, G., Cafasso, D. (2018). The complete plastid  
381 genomes of *Ophrys iricolor* and *O. sphegodes* (Orchidaceae) and comparative analyses with other  
382 orchids. *PLOS ONE* 13, e0204174. doi.org/10.1371/journal.pone.0204174  
383
- 384 Ruhlman, T.A., Jansen, R.K. (2014). The plastid genomes of flowering plants. ‘Chloroplast  
385 Biotechnology’. *Methods Mol. Biol.* 3–38. doi.org/10.1007/978-1-62703-995-6\_1  
386
- 387 Sabater, B. (2021). On the edge of dispensability, the chloroplast *ndh* genes. *Int. J. Mol. Sci.* 22, 12505.  
388 doi.org/10.3390/ijms222212505  
389
- 390 Schelkunov, M.I., Shtratnikova, V.Y., Nuraliev, M.S., Selosse, M.A., Penin, A.A., Logacheva, M.D.  
391 (2015). Exploring the limits for reduction of plastid genomes: A case study of the mycoheterotrophic  
392 orchids *Epipogium aphyllum* and *Epipogium roseum*. *Genome Biol. Evol.* 7, 1179–1191.  
393 doi.org/10.1093/gbe/evv019  
394
- 395 Schlechter (1911). LII. *D. gracile* Schltr. nov. spec. in *Repertorium Specierum Novarum Regni*  
396 *Vegetabilis* 10: 191. Berlin, Selbstverlag des Herausgebers 1912[1911].  
397
- 398 Serna-Sánchez, M.A., Pérez-Escobar, O.A., Bogarín, D., Torres-Jimenez, M.F., Alvarez-Yela, A.C.,  
399 Arcila-Galvis, J.E., Hall, C.F., De Barros, F., Pinheiro, F., Dodsworth, S., Chase, M.W., Antonelli, A.,  
400 Arias, T. (2021). Plastid phylogenomics resolves ambiguous relationships within the orchid family and  
401 provides a solid timeframe for biogeography and macroevolution. *Sci. Rep.* 11, 6858.  
402 doi.org/10.1038/s41598-021-83664-5  
403
- 404 Suetsugu, K., Ohta, T., Tayasu, I. (2018). Partial mycoheterotrophy in the leafless orchid *Cymbidium*  
405 *macrorhizon*. *Am. J. Bot.* 105(9): 1595–1600. doi.org/10.1002/ajb2.1142  
406
- 407 Sun, Y., Moore, M.J., Lin, N., Adelalu, K.F., Meng, A., Jian, S., Yang, L., Li, J., Wang, H. (2017).  
408 Complete plastome sequencing of both living species of Circaeasteraceae (Ranunculales) reveals  
409 unusual rearrangements and the loss of the *ndh* gene family. *BMC Genom.* 9;18(1):592.  
410 doi.org/10.1186/s12864-017-3956-3  
411
- 412 Tamura, K., Stecher, G., Kumar, S. (2021). MEGA11: Molecular evolutionary Genetics Analysis  
413 Version 11 (FU Battistuzzi, Ed.). *Mol. Biol. Evol.* 38, 3022–3027. doi.org/10.1093/molbev/msab120  
414
- 415 Thode, V.A., Lohmann, L.G. (2019). Comparative chloroplast genomics at low taxonomic levels: A  
416 case study using *Amphilophium* (Bignoniaceae, Bignoniaceae). *Front. Plant Sci.* 10, 796.  
417 doi.org/10.3389/fpls.2019.00796  
418
- 419 Tu, X.D., Liu, D.K., Xu, S.W., Zhou, C.Y., Gao, X.Y., Zeng, M.Y., Zhang, S., Chen, J.L., Ma, L., Zhou,  
420 Z., Huang, M.Z., Chen, S.P., Liu, Z.J., Lan, S.R., Li, M.H. (2021). Plastid phylogenomics improves  
421 resolution of phylogenetic relationship in the *Cheirostylis* and *Goodyera* clades of Goodyerinae  
422 (Orchidoideae, Orchidaceae). *Mol. Phyl. Evol.* 164, 107269. doi.org/10.1016/j.ympev.2021.107269  
423
- 424 Wen, Y., Qin, Y., Shao, B., Li, J., Ma, C., Liu, Y., Yang, B., Jin, X. (2022). The extremely reduced,  
425 diverged and reconfigured plastomes of the largest mycoheterotrophic orchid lineage. *BMC Plant Biol.*  
426 22, 448 (2022). doi.org/10.1186/s12870-022-03836-x  
427

- 428 WFO (2023). World Flora Online. Available at: <http://www.worldfloraonline.org> (Accessed in  
429 September 2023)  
430
- 431 Wicke, S., Müller, K., De Pamphilis, C., Quandt, D., Bellot, S., Schneeweiss G (2016). Mechanistic  
432 model of evolutionary rate variation en route to a nonphotosynthetic lifestyle in plants. *Proc. Nat. Acad.*  
433 *Sci.* 113 (32), 9045–9050. doi.org/10.1073/pnas.1607576113  
434
- 435 Wicke, S., Naumann, J. (2018). Molecular evolution of plastid genomes in parasitic flowering plants.  
436 *Adv. Bot. Res.* 85, 315–347. doi.org/10.1016/bs.abr.2017.11.014  
437
- 438 Wu, S., Chen, J., Li, Y., Liu, A., Li, A., Yin, M., Shrestha, N., Liu, J., Ren, G. (2021). Extensive  
439 genomic rearrangements mediated by repetitive sequences in plastomes of *Medicago* and its relatives.  
440 *BMC Plant Biol.* 21, 421. doi.org/10.1186/s12870-021-03202-3  
441
- 442 Yamori, W., Shikanai, T., Makino, A. (2015). Photosystem I cyclic electron flow via chloroplast NADH  
443 dehydrogenase-like complex performs a physiological role for photosynthesis at low light. *Sci. Rep.* 5,  
444 13908. doi.org/10.1038/srep13908  
445
- 446 Yang, J.B., Tang, M., Li, H.T., Zhang, Z.R., Li, D.Z. (2013). Complete chloroplast genome of the genus  
447 *Cymbidium*: lights into the species identification, phylogenetic implications and population genetic  
448 analyses. *BMC Evol. Biol.* 13, 84. doi.org/10.1186/1471-2148-13-84  
449
- 450 Yule, G.U. (1925). A mathematical theory of evolution, based on the conclusions of Dr. J. C. Willis,  
451 F.R.S. *Philos. Trans. R. Soc. B Biol. Sci.* 213, 21–87. doi:10.1098/rstb.1925.0002  
452
- 453 Zhang, G., Hu, Y., Huang, M.Z., Huang, W.C., Liu, D.K., Zhang, D., Hu, H., Downing, J.L., Liu, Z.J.,  
454 Ma, H. (2023). Comprehensive phylogenetic analyses of Orchidaceae using nuclear genes and  
455 evolutionary insights into epiphytism. *J. Integr. Plant Biol.* 65(5), 1204–1225.  
456 doi.org/10.1111/jipb.13462  
457
- 458 Zuckerkandl, E., Pauling, L. (1965). Molecules as documents of evolutionary history. *J. Theor. Biol.* 8,  
459 357–366.